Reviews in Mineralogy & Geochemistry
Vol. 86 pp. 291–322, 2021

Triple Oxygen Isotope Variations in Earth's Crust

Daniel Herwartz
Institut für Geologie und Mineralogie
Universität zu Köln
Zülpicher Str. 49b
50674 Cologne
Germany
d.herwartz@uni-koeln.de

INTRODUCTION

Analyzing classic $^{18}O/^{16}O$ ratios in solids, liquids and gases has proven useful in almost every branch of earth science. As reviewed in this book, additional ^{17}O analysis generally help to better constrain the underlying fractionation mechanisms providing a more solid basis to quantify geologic processes. Mass independent fractionation (MIF) effects known from meteorites and atmospheric gases (Clayton et al. 1973; Thiemens and Heidenreich 1983; Thiemens and Lin 2021, this volume; Brinjikji and Lyons 2021, this volume) generate large ^{17}O anomalies (expressed as $\Delta^{17}O$) that can be transferred to solids (Bao 2015; Cao and Bao 2021, this volume; Pack 2021, this volume) and to Earth′s crust (Peters et al. 2020a). However, such occurrences are rarely observed in igneous or metamorphic rocks. Most of the literature summarized herein, deals with much smaller ^{17}O "anomalies" stemming from fundamental differences between individual mass dependent fractionation mechanisms (e.g., equilibrium vs. kinetic isotope fractionation) and mixing processes. The basic theory for these purely mass dependent triple oxygen isotope fractionation mechanisms is long known (Matsuhisa et al. 1978; Young et al. 2002), but respective applications require high precision isotope analysis techniques that are now available for a number of materials including silicates, sulfates, carbonates and water.

Clear differences between equilibrium and kinetic isotope fractionation effects resolved for water (Barkan and Luz 2005, 2007) triggered novel research related to the meteoric water cycle, where the "$^{17}O_{excess}$ parameter" is introduced in analogy to the traditional "D_{excess} parameter" (Surma et al. 2021, this volume). Both D_{excess} and $^{17}O_{excess}$ (= $\Delta'^{17}O$ herein) are defined such that they remain more or less constant for equilibrium fractionation and evolve if kinetic processes occur. Triple oxygen isotope systematics in the meteoric water cycle are therefore similar to δD vs. $\delta^{18}O$ systematics, but with some important differences (Landais et al. 2012; Li et al. 2015; Surma et al. 2018, Voigt et al. 2020). Chemical precipitates or alteration products capture and preserve the triple oxygen isotopic composition of ambient water as shown for gypsum (Herwartz et al. 2017; Gázquez et al. 2018; Evans et al. 2018), silicates (Pack and Herwartz 2014; Levin et al. 2014; Sharp et al. 2016; Wostbrock et al. 2018; Wostbrock and Sharp 2021, this volume), weathering products (Bindeman 2021, this volume) and carbonates (Passey et al. 2014; Passey and Levin 2021, this volume;). Most studies focus on low *T* environments, were fractionation factors are large and kinetic effects as well as mixing can be important generating significant variability in $\Delta'^{17}O$ due to purely mass dependent effects.

In igneous or metamorphic systems, temperatures are high and timescales are sufficiently long to attain equilibrium. Hence, variability in $\Delta'^{17}O$ should be limited. Indeed, abundant high precision analyses of peridotites and primitive mantle melts reveal no obvious variability in $\Delta'^{17}O$

1529-6466/21/0086-0009$05.00 (print)
1943-2666/21/0086-0009$05.00 (online)
http://dx.doi.org/10.2138/rmg.2021.86.09

(Wiechert 2001; Spicuzza et al. 2007; Hallis et al. 2010; Tanaka and Nakamura 2013; Pack and Herwartz 2014; Herwartz et al. 2014; Young et al. 2016; Starkey et al. 2016; Cano et al. 2020). The exception are rocks that have interacted with water. The triple oxygen isotopic composition of surface water is generally distinct from the rocks and minerals they interact with (Tanaka and Nakamura 2013) and water partially transfers its isotopic composition to the alteration products. The original water isotopic composition can be calculated from hydrothermally altered rocks providing a tool to study paleo hydrology (Chamberlain et al. 2020) including Precambrian seawater (Zakharov and Bindeman 2019; Peters et al. 2020b) and ancient glacial water from snowball Earth episodes (Herwartz et al. 2015; Zakharov et al. 2017, 2019a)

Compared to the low *T* applications, the field of triple oxygen isotopes in high *T* environments is young, partly owing to the fact that "anomalies" in $\Delta'^{17}O$ are more difficult to resolve, when fractionation in $^{18}O/^{16}O$ is limited. The set of recent papers summarized herein demonstrates the potential of triple oxygen isotope systematics in hydrothermally altered, igneous and metamorphic rocks. The next pages introduce the basics of triple oxygen isotope systematics with a focus on purely mass dependent processes. I will then review a classic experimental concept to acquire equilibrium fractionation factors using triple oxygen isotopes before focusing on water–rock interaction and individual processes such as assimilation, dehydration and decarbonation that can be traced via triple oxygen isotope systematics. Finally, I will discuss alteration using an exotic example of lunar meteorite finds weathered in dry desert environments.

GUIDING PRINCIPALS

The theoretical framework for isotope fractionation on a quantum mechanical level was set by Urey, Bigeleisen and Mayer demonstrating how chemical bond strength and temperature control isotope fractionation, something widely known as "equilibrium isotope fractionation" today (Bigeleisen and Mayer 1947; Urey 1947; Yeung and Hayles 2021, this volume; Schauble and Young 2021, this volume). Isotopic discrimination between two substances generally increases with decreasing temperature, providing the basis for isotope paleo-thermometers ranging from the traditional $^{18}O/^{16}O$ carbonate paleo-thermometer (Epstein et al. 1951; Epstein and Mayeda 1953), to a wide range of mineral–mineral thermometers used in earth sciences (Matthews 1994). The respective isotopic temperature estimates are only accurate if equilibrium between the isotopic substances is attained. Any deviation from equilibrium (e.g., due to kinetic effects, alteration or mixing) compromises temperature accuracy.

The term "kinetic isotope fractionation" is used in various ways, sometimes addressing diffusion, or the preferential breaking of chemical bonds with light isotopes, and sometimes simply meaning that equilibrium is not attained. Besides insufficient time to reach equilibrium, isotopic fluxes between reservoirs can hold individual reservoirs in a steady state (e.g., seawater; Pack and Herwartz 2014), leading to apparent fractionation factors that are unrelated to thermodynamic equilibrium between two phases. These various types of "kinetic isotope fractionation" can be distinguished because the underlying physics dictate characteristic slopes in triple oxygen isotope space, all of which differ from equilibrium. This offers an elegant way of identifying kinetic processes and thus allows testing the equilibrium assumption.

Physical transport processes critically control effective isotopic fractionation between individual reservoirs (Druhan et al. 2019). Simple mathematical models such as batch or open system Rayleigh fractionation are often used to approximate isotopic fractionation curves, but considerable complexity is expected and observed in nature (Dansgaard 1964; Druhan et al. 2019). Even simple batch experiments designed to constrain equilibrium fractionation factors can show artefacts of intra-experiment transport processes and kinetic isotope effects (Matsuhisa et al. 1978).

With a single isotope ratio, it is challenging to: 1) identify complex transport mechanisms; 2) verify equilibrium; or 3) to pinpoint superimposed kinetic effects or a mixing process. The characteristic slopes and curves in triple oxygen isotope space allow to identify and sometimes to quantify a given combination of fractionation processes. The diverse applications summarized in this book demonstrate the versatile nature of additional $^{17}O/^{16}O$ analyses to the traditional $^{18}O/^{16}O$ isotope system.

Definitions, reference frames and the significance of TFL′s, MWL′s and θ

Quantification of triple oxygen isotope fractionation builds on traditional notations. Isotope ratios are reported in the traditionally delta notation (Eqn. 1) relative to an international standard. For oxygen:

$$\delta^i O = \frac{{}^iR_{\text{sample}} - {}^iR_{\text{reference}}}{{}^iR_{\text{reference}}} \quad (1)$$

where "R" stands for the ratio of the rare isotope "*i*" (17 or 18) relative to the abundance of ^{16}O. Fractionation between two phases A and B is quantified via the ratio of the isotope ratios:

$$\alpha^{i/16}_{\text{A-B}} = \frac{{}^iR_A}{{}^iR_B}\frac{1+\delta^i O_A}{1+\delta^i O_B} \quad (2)$$

and both fractionation factors are related by:

$$\alpha^{17/16}_{\text{A-B}} = \left(\alpha^{18/16}_{\text{A-B}}\right)^{\theta} \quad (3)$$

The key observation is that θ is not constant, but somewhat dependent on the fractionation process (mainly kinetic vs. equilibrium) and to a lesser extent on the substances involved, as well as fractionation temperature (Fig. 1). Therefore, the $\delta^{17}O$ is expected to vary as a function of θ, and thus with the fractionation process.

To visualize the small $^{17}O/^{16}O$ variations, the $\Delta'^{17}O$ (or $^{17}O_{excess}$) notation is used, which quantifies the deviation from an arbitrary reference slope (λ).

$$\Delta'^{17}O = \delta'^{17}O - \lambda \times \delta'^{18}O \quad (4)$$

Here, λ = 0.528 is used as a reference slope so that $\Delta'^{17}O = {}^{17}O_{excess}$ (see below). In this logarithmic form of the delta notation, with:

$$\delta'^i O = \ln\left(1+\delta^i O\right) \quad (5)$$

processes follow lines, while they would represent curves in the traditional $\delta^{18}O$ vs. $\delta^{17}O$ space. Mixing lines, however, which are linear in $\delta^{18}O$ vs. $\delta^{17}O$ space represent curves in the δ′ reference frame.

Reservoirs A and B in Figure 2 are in equilibrium at a given temperature. The fractionation of $^{18}O/^{16}O$ and $^{17}O/^{16}O$ are represented by the $1000\ln{}^{18}\alpha_{eq}$ and $1000\ln{}^{17}\alpha_{eq}$, respectively. Hence, the slope connecting the two equilibrated phases in the δ′ reference frame is $\ln{}^{17}\alpha_{A\text{-}B} / \ln{}^{18}\alpha_{A\text{-}B}$, which is the definition of $\alpha_{A\text{-}B}$.

If this $\theta_{A\text{-}B}$ differs numerically from the reference slope λ, the $\Delta'^{17}O$ of phases A and B are not identical. As an example, phase A could be SMOW and thus part of the reference line and B could be SiO_2. The $\theta_{SiO_2\text{–water}} = 0.5245$ at 25°C (Sharp et al. 2016), hence lower than the reference slope chosen here (0.528). Therefore, SiO_2 in equilibrium with SMOW has a negative $\Delta'^{17}O$ (Fig. 2). If λ = 0.5245 was chosen as a reference slope, $\Delta'^{17}O$ would be zero. So-called 'Terrestrial Fractionation Lines′ (TFL) that are defined by regressions through

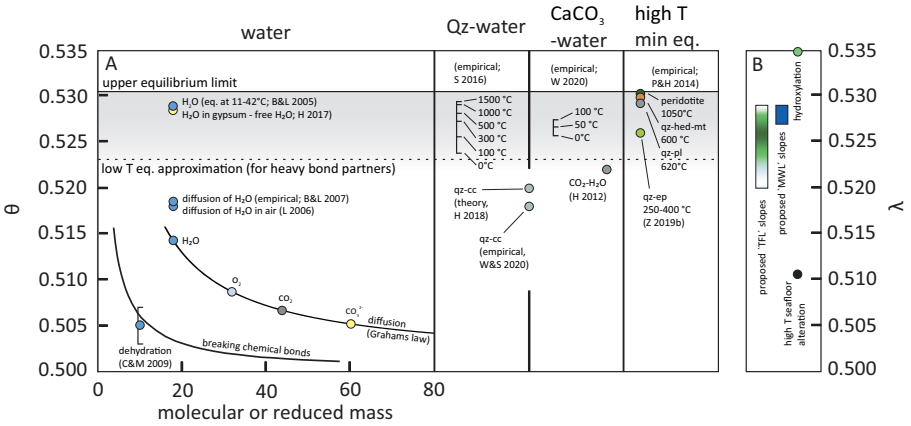

Figure 1. Selected triple oxygen isotope exponents (θ) for kinetic and equilibrium fractionation (**Panel A**) and resulting slopes (**Panel B**). **A)** The θ_{diff} for diffusion of molecules increases with decreasing molecular mass, as indicated by the solid black curve labeled "diffusion" (estimated using Grahams law). The lower limit for θ_{diff} is 0.5 for diffusion of oxygen bound to a molecule of infinite mass. Empirical and experimental constraints for θ_{diff} of water are 0.518 and 0.5185 (Landais et al. 2006; Barkan and Luz 2007). Breaking chemical bonds results in low θ_{kin} especially when the oxygen bond partner is heavy, but also for dehydration of serpentinite or brucite (Clayton and Mayeda 2009). The upper limit for θ_{eq} = 0.5305 at infinite temperature (Matsuhisa et al. 1978) and equilibrium often approaches θ_{eq} = 0.5232 at low temperatures (Dauphas and Schauble 2016; Hayles et al. 2018). Empirically determined θ_{eq} generally fall in this range as observed for liquid–vapor (Barkan and Luz 2005); gypsum–water (Herwartz et al. 2017; Gázquez et al. 2017; Liu et al. 2019); qz–water (Sharp et al. 2018; Wostbrock et al. 2018), cc–water (Wostbrock et al. 2020b) and high *T* mineral equilibria (Tanaka and Nakamura 2013; Pack and Herwartz 2014; Sharp et al. 2016; Zakharov et al. 2019b). However, both empirical and theoretical estimates for θ_{eq} of qz–cc are clearly lower than 0.5232 (Wostbrock and Sharp 2021, this volume; Hayles et al. 2018). The equilibrium $\theta_{CO_2–water}$ = 0.522 ± 0.002 (Hofmann et al. 2012) is lower, but within error identical to 0.5232. Empirical θ_{eq} estimates for carbonate–water (Voarintsoa et al. 2020) are lower than theoretical θ_{eq} estimates for carbonate–water (Cao and Liu 2011; Hayles et al. 2018), which are in turn lower than the empirical $\theta_{carbonate–water}$ calibration of Wostbrock et al. (2020b). These discrepancies are either related to kinetic effects during carbonate precipitation or to analytical artefacts. **B)** The effective TFL or MWL slopes (λ) vary depending on the sample suite used to define them. Therefore, respective λ values have restricted physical meaning. Note that effective λ can have values far outside the theoretical range as exemplified here for high *T* seafloor alteration with λ ≈ 0.51 (Pack and Herwartz 2014; Sengupta and Pack 2018; Zakharov et al. 2019b) and for hydroxylation λ ≈ 0.535 explained in the main text.

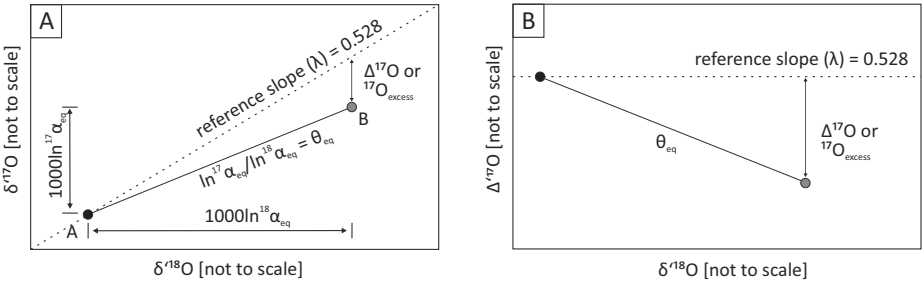

Figure 2. Isotope fractionation in triple isotope space. Materials A and B are in isotopic equilibrium with a triple isotope exponent θ lower than 0.528. Because the triple oxygen isotopic composition of A falls on the reference line ($\Delta'^{17}O = 0$), substance B comprises negative $\Delta'^{17}O$. The *x* and *y* axis in **panel A** are not to scale, as otherwise the deviation from the reference slope (**stippled line**) would not be visible. In the $\delta'^{18}O$ vs. $\Delta'^{17}O$ reference frame (**panel B**), which is commonly used to better visualize the small offsets from a reference slope in triple oxygen isotope space, the reference slope from **panel A** is a horizontal line ($\Delta'^{17}O = 0$).

unrelated terrestrial rocks often comprise values around 0.5245 (Pack et al. 2007; Rumble et al. 2007). These TFL slopes typically include quartz to define the high $\delta'^{18}O$ region of TFL slopes, hence the numerical similarity of some TFL slopes and the empirical $\theta_{SiO_2-water}$ at low *T* is not a coincidence. Apart from this, the slopes of these suites of unrelated rock samples (TFL′s) have no meaning (Matsuhisa et al. 1978; Pack and Herwartz 2014, 2015).

Typical compositions of silicate rocks comprise negative $\Delta'^{17}O$ and are depleted relative to seawater $\Delta'^{17}O = -5$ ppm (i.e., −0.005‰) and meteoric water that cluster around the global meteoric water line, termed MWL with positive $\Delta'^{17}O$ (Luz and Barkan 2010; Tanaka and Nakamura 2013). Global compilations of meteoric water actually reveal curved relationships (Li et al. 2015; Sharp et al. 2018), hence the variation in published MWL slopes does not come unexpected and individual regression values are of limited significance.

A common MWL slope value of 0.528 is used as a reference slope to define $^{17}O_{excess}$ in the hydrological literature (Passey and Levin 2021, this volume; Surma et al. 2021, this volume). When dealing with water–rock interaction, it is convenient if $^{17}O_{excess} = \Delta'^{17}O$. Hence, it makes sense to use the same reference slope ($\lambda = 0.528$ is always used for $^{17}O_{excess}$) to define $\Delta'^{17}O$. Both water and rocks should be reported on SMOW-SLAP scale (Schoenemann et al. 2013; Sharp and Wostbrock 2021, this volume). Silicate samples are, however, measured relative to rock standards (San Carlos Olivine, NBS28, UWG, etc.) and respective calibrations to SMOW-SLAP scale differ by about 24 ppm on average (Pack et al. 2016; Wostbrock et al. 2020a). Here, I use a mean estimate (Table 1) that agrees well with more comprehensive data compilations published in this volume (Miller and Pack 2020; Sharp and Wostbrock 2020). As demonstrated below, the choice of the scale can critically affect interpretations of water–rock interaction studies.

The intercalibration of two non-identical materials (e.g., silicates vs. water) is challenging because non-identical methods are required for their analyses resulting in non-identical blanks and matrix effects. Even for the same material cross contamination, pressure baseline effects and effects tied to the design of mass spectrometers can result in scale distortion between laboratories that can be easily corrected if two standard materials are routinely analyzed (Schoenemann et al. 2013; Yeung et al. 2018). Miller et al. (2020) now provides two rock standards namely SKFS (Stevns Klint Flint Standard with $\delta^{18}O = 33.8$‰) and KRS (Khitostrov Rock Standard with $\delta^{18}O = -25.02$‰) that are far removed from each other and are thus ideal for scaling (most SMOW-SLAP calibrated KRS and SKFS data is given in Sharp and Wostbrock 2021, this volume). The same concept can be used for carbonates e.g., by using the recent calibration of NBS18 and NBS19 (Wostbrock et al. 2020a). Data reported herein is mostly SMOW-SLAP scaled by applying shifting and scaling factors of Pack et al. (2016) to older data from Göttingen. Ilya Bindeman kindly provided KRS and SKFS analyses that I used to bring all published data from their lab to the same scale (Table 1).

Mass dependent isotope fractionation in triple oxygen isotope space

Both $^{18}\alpha_{eq}$ and $^{17}\alpha_{eq}$ decrease with increasing temperature, while θ_{eq} increases with increasing temperature. Therefore, equilibrated phases fall on the respective equilibrium curve in triple oxygen isotope space (Fig. 3). Deviation from this "equilibrium curve" indicates disequilibrium.

Equilibrium fractionation factors generally range between $\theta = 0.5232$ and 0.5305 (Matsuhisa et al. 1978; Young et al. 2002; Cao and Liu 2011; Dauphas and Schauble 2016; Hayles et al. 2016) The upper limit for equilibrium fractionation at infinite temperature is $\theta = 0.53052$ and defined by:

$$\theta = \frac{\frac{1}{m_1} - \frac{1}{m_2}}{\frac{1}{m_1} - \frac{1}{m_3}} \tag{6}$$

where the m_1 (15.9949146), m_2 (16.9991315) and m_3 (17.9991604) correspond to the isotopic masses of ^{16}O, ^{17}O and ^{18}O. For heavy bond partners, the low T approximation for θ often approaches:

$$\theta = \frac{\sqrt{\frac{1}{m_1}} - \sqrt{\frac{1}{m_2}}}{\sqrt{\frac{1}{m_1}} - \sqrt{\frac{1}{m_3}}} \quad (7)$$

and thus 0.52316 (Hayles et al. 2016; Dauphas and Schauble 2016). The grey field in Figure 1 covers most of the θ_{eq} values that are expected to occur in nature, but the lower boundary is not strict and there are equilibrium θ such as the qz–cc equilibrium (Wostbrock and Sharp 2021, this volume) that are clearly lower than predicted by Equation (7). For materials that mainly comprise hydrogen as a bonding partner to oxygen θ_{eq} are generally high (Dauphas and Schauble 2016). The high vibrational frequencies of O–H bonds lead to high θ for water–vapor equilibrium even at low temperatures as confirmed empirically for water $\theta_{liquid-vapor} = 0.529$ in the 11 to 42°C temperature range (Barkan and Luz 2005). For very small $\alpha_{A\text{-}B}$, apparent θ far outside the theoretical limits of 0.5 to 0.5305 may apply (Bao et al. 2015; Hayles et al. 2016).

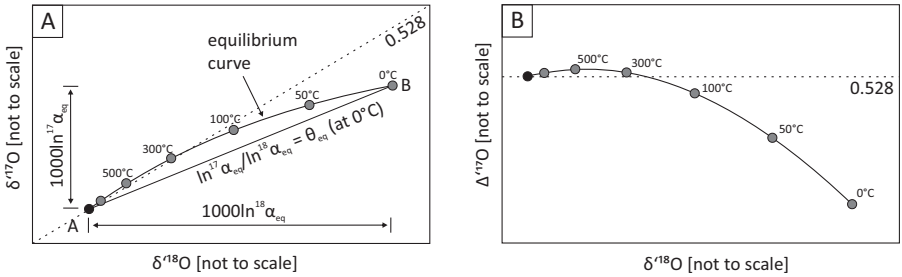

Figure 3. Equilibrium isotope fractionation between substances A and B at variable temperatures. Due to the small temperature dependency of θ, equilibrium in triple oxygen isotope space is represented by the **black curves** in both panels.

Graham′s law provides a first order approximation for diffusion (Young et al. 2002). The relative velocities of diffusing species are directly proportional to their molecular mass so that:

$$\theta_{diff} = \frac{\ln\left(\frac{m_1}{m_2}\right)}{\ln\left(\frac{m_1}{m_3}\right)} \quad (8)$$

where m_1, m_2 and m_3 correspond to the isotopologues comprising ^{16}O, ^{17}O and ^{18}O respectively, giving $\theta_{diff} = 0.5142$ for individual H_2O molecules (Fig. 1). The details of diffusion are more complex leading to slightly higher theoretical $\theta_{diff} = 0.518$ for diffusion in air, which is very close to the empirical estimate of $\theta_{diff} = 0.5185$ (Barkan and Luz 2007; Landais et al. 2006). Other kinetic processes such as the preferential breaking of bonds comprising light isotopes scale with the reduced mass of the bond partners so that θ_{kin} for bond breaking differs from θ_{diff} (Fig. 1). Beyond Grahams law, the prediction of θ_{kin} can be challenging. Transition state theory considers that chemical reactions generally proceed via transitional states (Bigeleisen and Wolfsberg 1958). Consider a phase A with a transition state $A^{\ddagger}$ that reacts to phase B.

$$A \leftrightharpoons A^{\ddagger} \rightarrow B \quad (9)$$

Table 1. Reference frame: A wide range of studies calibrate rock standards to SMOW but absolute values differ beyond analytical precision, including recent calibrations of silicate standards and air O_2 on a SMOW-SLAP scale (Pack et al. 2016; Wostbrock et al. 2020a). Here I use an intermediate scale calculated by simply adding or subtracting 12 ppm (the average offset between SCO, NBS28 and UWG is ca. 24 ppm) to standard data of Pack et al. (2016) and Wostbrok et al. (2020a). The mean values compare well to previous calibrations (e.g., SCO from Sharp et al. 2016) and considerably reduces the offset for AIR O_2 between the two labs. These average values are almost identical to the more comprehensive compilation by Sharp and Wostbrock (2020) in this volume. I recommend using the later in future studies.

Material/Reference	Shifted by:	$\delta^{17}O$	SD	$\delta^{18}O$	SD	$\Delta'^{17}O_{(0.528)}$	SD
SC Olivine							
Pack et al. 2016 (GZG)	$\delta'^{17}O - 0.012$	2.668		5.152		−49	
Pack et al. 2016 (ISI)	$\delta'^{17}O - 0.012$	2.737		5.287		−51	
Sharp et al. 2016	$\delta'^{17}O$	2.745		5.310		−55	
Wostbrock et al. 2020a	$\delta'^{17}O + 0.012$	2.732		5.268		−46	
mean		2.72	0.04	5.25	0.07	−50	4
mean in S&W 2020		2.75	0.08	5.32	0.16	−52	14
UWG−2							
Miller et al. 2019 (GZG)	$\delta'^{17}O - 0.012$	2.974		5.750		−58	
Miller et al. 2019 (OU)	$\delta'^{17}O - 0.012$	2.974		5.750		−58	
Wostbrock et al. 2020a	$\delta'^{17}O + 0.012$	2.944		5.696		−59	
mean		2.96	0.02	5.73	0.03	−58	1
mean in S&W 2020		2.94	0.08	5.70		−64	
NBS28							
Miller et al. 2019 (GZG)	$\delta'^{17}O - 0.012$	4.927		9.452		−52	
Miller et al. 2019 (OU)	$\delta'^{17}O - 0.012$	4.997		9.555		−37	
Wostbrock et al. 2020a	$\delta'^{17}O + 0.012$	4.998		9.577		−47	
Pack et al. 2017	$\delta'^{17}O - 0.012$	5.074		9.712		−42	
mean		5.00	0.06	9.73	0.11	−45	7
mean in S&W 2020		4.99		9.57		−49	
KRS							
Miller et al. 2019 (GZG)	$\delta'^{17}O - 0.012$	−13.307		−24.899		−83	
Miller et al. 2019 (OU)	$\delta'^{17}O - 0.012$	−13.465		−25.200		−80	
mean		−13.386	0.112	−25.050	0.213	−82	2
mean in S&W 2020		−13.381		−25.023		−91	
SKFS							
Miller et al. 2019 (GZG)	$\delta'^{17}O - 0.012$	17.410		33.477		−126	
Miller et al. 2019 (OU)	$\delta'^{17}O - 0.012$	17.646		33.932		−127	
mean		17.528	0.167	33.705	0.322	−127	0
mean in S&W 2020		17.556		33.778		−137	
AIR							
Pack et al. 2017 – 12ppm	$\delta'^{17}O - 0.012$	12.253		24.150		−421	
Wostbrock et al. 2020a 12ppm	$\delta'^{17}O + 0.012$	12.190		24.046		−430	
mean		12.221	0.044	24.098	0.074	−425	6
mean in S&W 2020		12.204	0.060	24.077	0.070	−432	24

Because transition states ($A^{\ddagger}$) are generally not observed and cannot be easily identified such a reaction may appear like a purely kinetic reaction from A to B. The combination of the two individual reactions with variable α's, however, can produce effective θ_{eff} outside the theoretical range. Most kinetic isotope reactions will be combinations of various physical processes resulting in variable approximations for isotope effects (Melander and Saunders 1980). Accurate predictions of θ_{kin} may serve as a tool to study the underlying physics of kinetic effects (Cao and Bao 2017; Yeung and Hayles 2021, this volume).

The term "kinetic isotope effect" is also frequently used to say that equilibrium is not attained, but the underlying processes remain unclear. Using carbonate formation at high pH and low temperature (25 °C), I will exemplify how a "kinetic isotope effect" can be a combination of mixing, diffusion and equilibration resulting in an effective slope (λ) in triple oxygen isotope space that is outside the theoretical range for θ (Fig. 4). Consider hydroxylation ($CO_2 + OH^- \rightarrow HCO_3^-$) as the rate limiting step for the subsequent precipitation of calcite. In equilibrium with water, the two reactants have vastly different oxygen isotopic compositions with $\delta^{18}O_{OH^-} = -38.4‰$ at 25°C (Green and Taube 1963) and $\delta^{18}O_{CO_2} \approx +40.5‰$ (Beck et al. 2005). A simple mass balance with $\delta^{18}O_{HCO_3^-} = 2/3\ \delta^{18}O_{CO_2} + 1/3\ \delta^{18}O_{OH^-}$ approximates the overall isotope effect in $\delta^{18}O$ for hydroxylation (Clark et al. 1992; Dietzel et al. 1992) resulting in $\delta^{18}O_{HCO_3^-} = 14.2‰$. In triple oxygen isotope space, this mixing product (HCO_3^-) falls on a mixing curve between CO_2 and OH^- resulting in a very low $\Delta'^{17}O_{HCO_3^-}$ of −286 ppm (Fig. 4B). Due to a superimposed kinetic isotope effect (Devriendt et al. 2017; Sade et al. 2020), the actual kinetic $CaCO_3$ hydroxylation endmember has a $\delta^{18}O_{CaCO3} \approx 10‰$ (Böttcher et al. 2018), so that the expected $\Delta'^{17}O_{CaCO_3} \approx -227$ ppm (using $\theta_{KIE} = 0.5143$ for a 4‰ kinetic effect). The mixing curve between this kinetic $CaCO_3$ hydroxylation endmember and $CaCO_3$ in full equilibrium defines an apparent kinetic fractionation curve with a slope $\lambda \approx 0.535$ (green arrow labeled "hydroxylation" in Fig. 4), even higher than the upper theoretical limit for equilibrium fractionation.

Using a numerical approach, Guo and Zhou (2019) show how disequilibrium causes departure from equilibrium in all directions depending on the underlying process(es) These perturbations of equilibrium actually form tight loops. The respective kinetic θ_{kin} are not generally restricted to low values as implied by Figure 1. For a combination of processes (e.g., equilibrium + kinetic + mixing in the above example), the notation λ_{kin} may be more appropriate than θ_{kin}.

Disequilibrium is common in carbonates (Coplen 2007; Daëron et al. 2019; Bajnai et al. 2020). Carbonate thermometry only works because the empirical $\delta^{18}O - T$ calibrations for a given carbonate material include "kinetic effects" (often termed "vital effects" for biogenic carbonates) as constant offsets from true equilibrium (Coplen 2007). Most Earth surface carbonates precipitate out of equilibrium (Daëron et al. 2019), hence disequilibrium is also expected at elevated temperatures especially when precipitation rates or pH are high (Guo and Zhou 2019). High precision carbonate $\Delta'^{17}O$ analyses are challenging, however, and first applications are only beginning to emerge for low T precipitates (Bergel et al. 2020; Wostbrock and Sharp 2021, this volume; Passey and Levin 2021, this volume).

Mixing

Mixing occurs at all scales. Consider: 1) the above example of hydroxylation for mixing on the molecular scale both for "$CO_2 + OH^-$" and "$CaCO_3$ in eq. + kinetic $CaCO_3$ endmember"; 2) mixing of evaporated water with unevaporated groundwater or precipitation in desert lake systems (Herwartz et al. 2017; Voigt et al. 2020); 3) intra mineral mixing of phytolith SiO_2 precipitated in leaves from water with variably evaporitic compositions (Alexandre et al. 2019); 4) intra mineral mixing of two quartz generations formed at opposing temperatures and water to rock ratios (Zakharov and Bindeman 2019; Zakharov et al. 2019a);

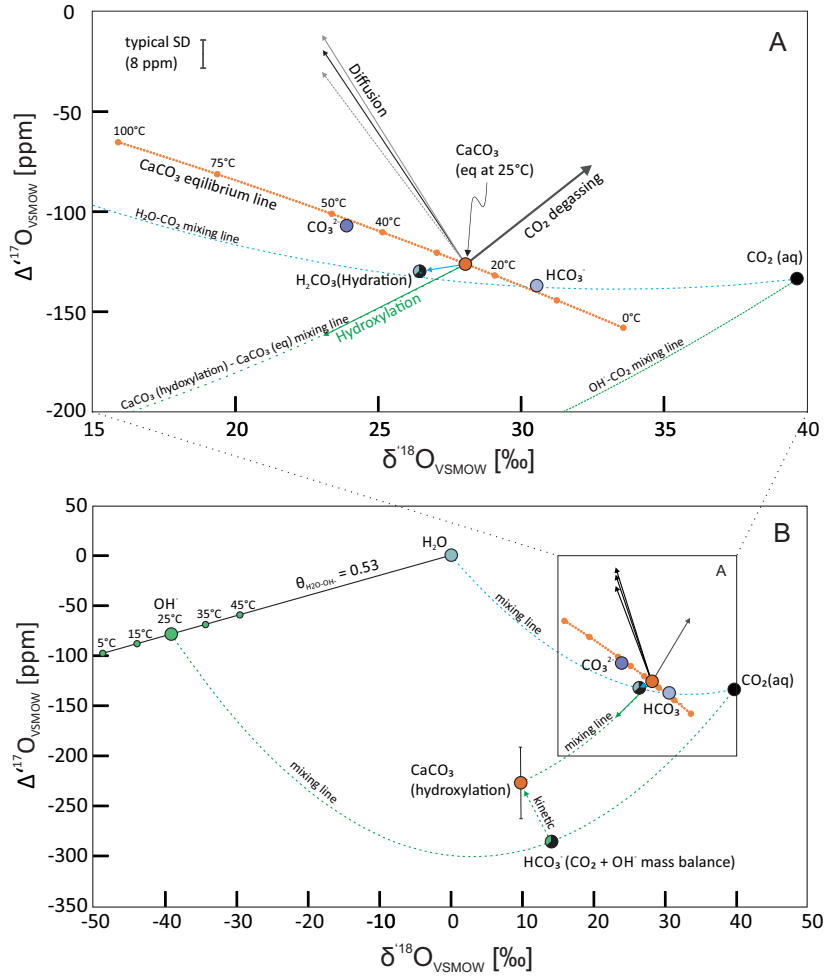

Figure 4. Illustration of predicted effective slopes in triple oxygen isotope space (i.e., $\delta'^{18}O$ vs. $\Delta'^{17}O$). In this reference space mixing lines fall on curves, while isotope fractionation processes are linearized. **Panel A:** The **stippled orange line** represents equilibrium fractionation of $CaCO_3$ at the given temperatures. This line and the equilibrium values for CO_3^{2-}, HCO_3^-, CO_2 (aq) at 25°C are estimated from published $\delta^{18}O$ vs. T (Kim and O'Neil 1997; Beck et al. 2005) and θ vs. T (Cao and Liu 2011) relationships. Kinetic effects drive samples away from this equilibrium curve. **Black and grey arrows**, for example, depict expected slopes for diffusion of CO_3^{2-} or HCO_3^- (θ_{diff} = 0.5052; **solid gray**) and CO_2 (θ_{diff} = 0.5066; **black**) using Grahams law; and for diffusion of CO_2 in air (θ_{diff} = 0.5098; **stippled gray**) using the equations given in Landais et al. (2006). The vector for CO_2 degassing (**thick black arrow**) is taken form Gou and Zhou (2019). Natural samples affected by hydration or hydroxylation are expected to fall on mixing lines between fully equilibrated $CaCO_3$ endmember and the respective kinetic endmembers (see **Panel B** and text for details). For hydration, the mass balance is: $\delta^{18}O_{H_2CO_3} = 2/3\ \delta^{18}O_{CO_2} + 1/3\ \delta^{18}O_{H_2O}$. At 25°C the $\delta^{18}O_{H_2CO_3}$ of this mixture is 27‰. The quantum mechanical estimates for the superimposed KIE of hydration (Zeebe 2014) is on the order of 1‰ or less relative to this mass balance (Devriendt et al. 2017). Quantitatively transformation to $CaCO_3$ results in a hydration endmember with only 2.5 per mill lower $\delta^{18}O_{CaCO3} \approx 26‰$ than the (presumed) equilibrium value of $\delta^{18}O_{CaCO_3}$ = 28.5 at 25°C (Kim and O'Neil 1997). The $\Delta^{17}O_{CaCO_3}$ would be = −130 ppm and the slope ≈ 0.533 (**short blue arrow** in panel A resembling mixing between "H_2CO_3 hydration" and "$CaCO_3$ eq. at 25°C"). The mass balance for hydroxylation is outlined in the main text (and illustrated in **Panel B**). The estimates for triple oxygen isotope slopes critically rely on the accuracy of the oxygen isotope fractionation factors. Using different literature values (e.g., Hofmann et al. 2012 for $\theta_{CO_2-water}$; Hayles et al. 2018 or Wostbrock et al. 2020b for $\theta_{CaCO_3-water}$; or Coplen et al. 2007 for $1000\ln^{18}\alpha_{CaCO_3-water}$) will substantially change estimated slopes e.g., for hydroxylation. This is a simplified conceptional figure.

5) mixing on the intra sample scale for metamorphic BIF′s (Levin et al. 2014); 6) intra sample mixing of pristine MORB and the alteration product clay (Pack and Herwartz 2014); 7) assimilation of altered rocks in magma chambers (Zakharov 2019b; Peters et al. 2020a); and 8) water–rock interaction (Herwartz et al. 2015). All of these mixing processes result in low $\Delta'^{17}O$ isotopic compositions in the mixing products. The further apart the mixing endmembers are in $\delta^{18}O$, the lower the resulting $\Delta'^{17}O$.

On a rock scale, minerals with contrasting isotopic compositions can isotopically mix and re-equilibrate. In a conceptual model, Levin et al. (2014) envisioned the precipitation of quartz and an Fe phase from ocean water at low temperature. Due to the small α_{eq} for FeO_x–water, the respective $\Delta'^{17}O_{FeOx}$ is always close to that of the initial water (whatever the θ; Fig. 5), while the $\Delta'^{17}O_{quartz} = -132$ ppm for precipitation at 25°C (with $\theta_{SiO_2-water} = 0.5243$; Sharp et al. 2016; Wostbrock et al. 2018). When this bi-mineralic rock is metamorphosed (with $T > 600$ °C), quartz and the iron phase re-equilibrate to high T conditions. The final $\Delta'^{17}O$ compositions fall close to the molar mean of the system, which lies on a concave mixing curve (Fig. 5). The model elegantly explains the apparently "too low" $\Delta'^{17}O$ of some (metamorphosed) banded iron formations (Levin et al. 2014) as well as the bulk composition of a metamorphosed BIF where the mineral separates (qz, hed, mt) re-equilibrated to a final $\theta_{qz-hed-mt} = 0.53$ at 600 °C (Pack and Herwartz 2014).

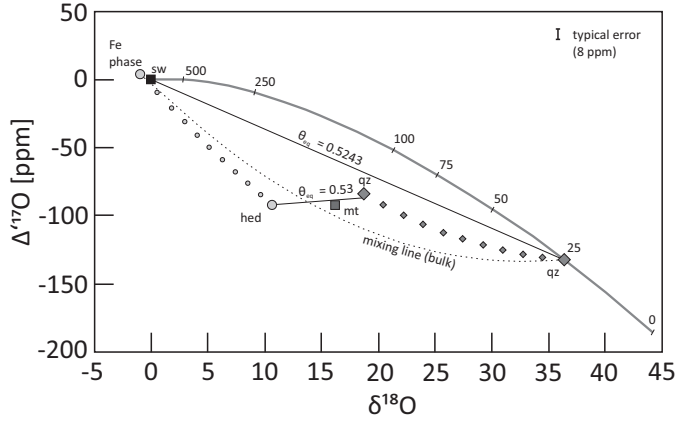

Figure 5. Model of intra-sample re-equilibration modified after Levin et al. (2014). Metamorphic BIF data from Pack and Herwartz (2014) is recalibrated to SMOW-SLAP scale. Numbers close to tick marks represent equilibrium temperatures for the qz–water system (Sharp et al. 2016).

Silicate rocks generally comprise positive $\delta^{18}O$ and negative $\Delta'^{17}O$, distinct from surface water leading to resolvable mixing relationships in hydrothermal settings (Fig. 6). The pristine water mixing endmember can be constrained even after the altered rocks have been metamorphosed (Herwartz et al. 2015). Hydrothermally altered rocks, as well as sediments such as carbonates, cherts, or clays comprise typical triple oxygen isotope compositions that can be traced when involved in metamorphic or magmatic processes (Peters et al. 2020a) ultimately leading to small heterogeneities in $\Delta'^{17}O$ expected between mantle melts (Cao et al. 2019).

The guiding principles outlined above allow: 1) to identify disequilibrium; 2) to distinguish between various types of kinetic effects; and 3) to identify mixing processes. Here, I focus on publications that apply these principals to solve geological problems.

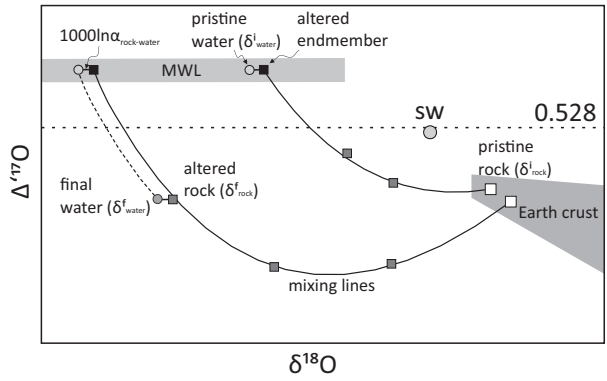

Figure 6. Mixing lines between crustal rocks (**gray shaded area**) and low $\delta^{18}O$ meteoric water (MWL) represent curves. The bulk triple oxygen isotopic composition of altered rock samples represents a mixture between these two reservoirs and falls on respective mixing lines. Details of this approach are explained in the main text.

QUANTIFYING FRACTIONATION FACTORS

As for the classic $^{18}\alpha_{A\text{-}B}$, temperature dependent fractionation factors for $^{17}\alpha_{A\text{-}B}$ and thus $\theta_{A\text{-}B}$ can be determined via modelling, by analyzing natural materials with known formation temperatures or from laboratory experiments. Equilibration timescales in experiments are always short compared to geological timescales. The two directional approach (Clayton et al. 1972) and the three-isotope method (Matsuhisa et al. 1978; Matthews et al. 1983) permit estimating equilibrium fractionation factors from unequilibrated batch type experiments, circumventing the problem of long timescales.

The two directional approach

The substances of interest are enclosed in sealed containers and left to equilibrate for variable periods of time, so that a time-series curve approaching equilibrium can be constructed for batches with identical starting composition. One experimental series comprises two or three combinations of starting compositions so that equilibrium is approached from two sides. Ideally, the respective curves converge to a single value representing equilibrium (Fig. 7A).

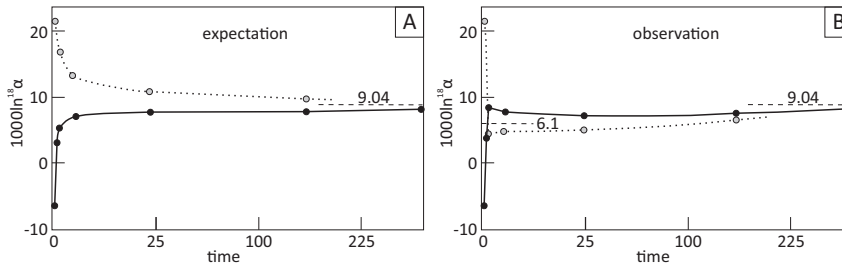

Figure 7. Two directional approach. **A)** In the idealized case, individual experiments fall on exponential curves that merge at the equilibrium $1000 \ln \alpha$. **Grey and black dots** represent expected values for equilibration between SiO_2 and water. **B)** In the real case example (with cristobalite as initial SiO_2 phase), the measured $1000 \ln \alpha$ fall on complex trajectories that are inconsistent with a gradual approach towards equilibrium (Matsuhisa et al. 1978).

It was soon realized that there can be complications with this approach. Clayton et al. (1972) warned that extrapolation can generate fractionation factors larger than the equilibrium value by 1 to 2‰, while Matsuhisa et al. (1978) observed fractionation factors 3‰ too low (Fig. 7B). Long standing inconsistencies between laboratories or between experiments and theory (Zheng 1993) reveal a certain degree of complexity within these apparently simple experiments. In principal, triple oxygen isotope systematics can now be used to test if experiments reached near equilibrium or not because theoretical $\theta_{A\text{-}B}$ estimates are more robust than estimates for classic ${}^{i}\alpha_{A\text{-}B}$ (Cao and Liu 2011; Hayles et al. 2018). In fact, a variety of this idea has been introduced long ago and is known as the "three-isotope method" (Matsuhisa et al. 1978).

The three-isotope method

The method requires two starting materials with different triple oxygen isotope compositions. Matsuhisa et al. (1978) produced water with extraordinary low $\Delta^{17}O$ by: 1) evaporating water to a point where the residual is extremely enriched with $\delta^{18}O$ = 6100‰; and 2) subsequent mixing with normal distilled water to final $\delta^{18}O$ compositions of 14.4 and 27.66‰ and very low $\Delta^{17}O$ of −5 and −7‰. Equal molar proportions of this low $\Delta^{17}O$ water and fine grained SiO_2 (quartz or cristobalite) are mixed and left to equilibrate at 250°C and 15 kbar in sealed platinum capsules. At full equilibrium quartz and water must fall on the same mass dependent fractionation line, that passes through the mass balance point of the closed system, the so called "secondary fractionation line". The original paper uses $\lambda = 0.52$ in $\delta^{18}O$ vs. $\delta^{17}O$ space, but for a more exact treatment 0.527 ($\theta_{qz\text{–}H_2O}$ at 250 °C; Sharp et al. 2016) should be used in $\delta'^{17}O$ vs. $\delta'^{18}O$ coordinates (Fig. 8). Even with only one single experiment it is possible to extrapolate from the initial isotopic compositions and the partially exchanged compositions to the final equilibrium value (Fig. 8A). Therefore, the triple isotope method is much less labor intensive than the two directional approach. The original result for $1000\ln{}^{18}\alpha_{SiO_2\text{–water}} = 9.03$‰ is remarkably consistent with the latest compilation of $1000\ln{}^{18}\alpha_{SiO_2\text{–water}} = 9.04$‰ at 250 °C (Sharp et al. 2016).

Even though the approach appears to be extremely elegant, Matsuhisa et al. (1978) demonstrate some limitations in the very same paper. In a second equilibration experiment, that utilized cristobalite instead of quartz as the initial SiO_2 phase, the measured quartz compositions cross the secondary equilibration line at apparently lower $1000\ln{}^{18}\alpha_{SiO_2\text{–waterr}} \approx 6.1$‰, overstep to apparently too low $\Delta'^{17}O_{quartz} < \Delta'^{17}O_{molar\ mean}$ and then slowly approach the equilibrium

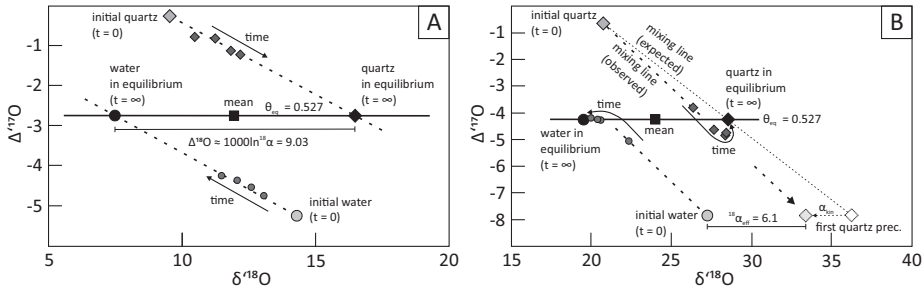

Figure 8. Three-isotope method. A) Idealized case with data from Experiment 1 of Matsuhisa et al. (1978). The secondary mass fractionation line with $\theta_{SiO_2\text{–water}} \approx 0.527$ (Sharp et al. 2016; Wostbrock et al. 2018) passes through the mean isotopic composition (**black diamond**). Water samples (**circles**) and quartz (**diamonds**) evolve towards their fully equilibrated endmembers (**black circle and diamond**) that can be approximated by linear regression (**stippled lines**). Curvature due to mixing is insignificant at this scale. **B)** Real case example with data from experiment 2 of Matsuhisa et al. (1978) using cristobalite instead of quartz as starting material. Symbols are equal to panel A. The **white diamond** represents the composition of initial quartz if precipitated in equilibrium (with $1000\ln{}^{18}\alpha_{qz\text{–water}} = 9.03$) with initial water (not supported by the data), while the **light gray diamond** indicates the composition of initial quartz if precipitated with a superimposed kinetic effect from initial water (supported by the data).

composition (Fig. 8B). At equimolar proportions of SiO_2 and water, only a small fraction of the cristobalite can dissolve, equilibrate with the water and re-precipitate as quartz (Bottinga and Javoy 1987). Therefore, the quartz formed at an early stage inherits a low $\Delta'^{17}O$ similar to the initial water (white diamond in Fig. 8B) resulting in the apparent overstepping of the measured quartz samples. The expected mixing line between such an early precipitate and the initial cristobalite crosses the secondary fractionation line at the equilibrium composition. Hence, low $\Delta'^{17}O$ quartz alone does not explain why regressions do not always pass through the equilibrium composition. About 50% of the cristobalite is transformed to quartz within the first three minutes (shortest experiment) and such fast reaction kinetics always hold potential for kinetic effects. The effective fractionation factor of $1000 \ln \alpha_{eff} = 6.1‰$ observed for the early experiment (as in the two directional approach; Fig. 7), shows that the initial SiO_2 reaction product did not form in equilibrium (Fig. 8). The initial "kinetic" quartz precipitates (light gray diamond in Fig. 8B) drive samples away from the expected re-equilibration trend. Samples from long experimental runs slowly approach full equilibrium due to slow re-equilibration of the initial quartz precipitates (also see Appendix 2 of Matsuhisa et al. 1978). These results show how even a seemingly simple batch experiment can result in inaccurate fractionation factor estimates if the underlying physics and transport mechanisms are not accounted for (Bottinga and Javoy 1987).

The three-isotope method is applied for oxygen and a range of other three-isotope systems (Matthews et al. 1983; Shahar et al. 2008, 2009; Beard et al. 2010; Lazar et al. 2012; Macris et al. 2013). A rigorous mathematical investigation (Cao and Bao 2017) using kinetic theory (Biegeleisen and Wolfsberg 1958) shows that accurate α_{eq} can only be determined if appropriate initial isotope compositions are chosen (Matthews et al. 1983) that minimize potential artefacts of the method. The main point of Cao and Bao (2017), however, is to show that re-equilibration trajectories do not necessarily follow linear slopes and that the form of these trajectories can be used to quantify kinetic isotope effects as crudely outlined above. Hence, the triple oxygen isotope method holds a greater potential than previously realized, providing a tool to tackle the complexity associated to open systems (Druhan et al. 2019), multiple reservoir exchange systems (Beard et al. 2010) and dissolution/re-precipitation (Putnis 2015).

The example of intra-rock mixing above (Fig. 5) demonstrates that the three-isotope method can now be used in natural systems. At the present analytical precision, the natural variability in initial $\Delta'^{17}O$ between two materials is often sufficient to apply the concept. Disequilibrium "frozen in" in multi component systems may eventually prove valuable to better understand and quantify the underlying kinetics (Cao and Bao 2017), which will be useful for the traditional concepts of "geothermometry" and "geospeedometry" (Clayton and Epstein 1961; Garlick and Epstein 1967; Dodson 1973; Giletti 1986).

Isotope thermometry and geospeedometry

The temperature dependence of equilibrium fractionation factors provide the basis to use coexisting minerals in magmatic and metamorphic rocks as geo-thermometers (Clayton and Epstein 1961; Garlick and Epstein 1967). Some mineral pairs, such as quartz and magnetite comprise relatively large $^{18}\alpha_{qz–mt}$ fractionation factors even at high T, due to the large difference in oxygen bond strength. The quartz–magnetite pair typically implies isotopic temperatures close to 600 °C for rocks that cooled fast, while at slow cooling rates the oxygen isotopes of the mineral pair can equilibrate to lower temperatures of around 550 °C (Dodson 1973). This concept of geospeedometry (Giletti 1986) can be applied to multi mineral assemblages with variable closure temperatures providing insight into exhumation and cooling of metamorphic rocks.

Some minerals are more susceptible to alteration than others, potentially leading to meaningless temperature estimates or exhumation rates. Alteration can be identified by comparing apparent equilibration (or closure) temperatures between several mineral pairs that should remain in feasible bounds for the presumed cooling rate of a simple p–T path. Aqueous fluids, however,

are known to enhance diffusion rates (Elphick and Graham 1988; Kohn 1999) making it challenging to decide if a given mineral pair is in equilibrium and thus if the isotopic temperatures are feasible. Late infiltration of water could either alter one individual mineral phase (e.g., magnetite or plagioclase) or facilitate equilibration between all phases at relatively low temperature.

By using triple oxygen isotope systematics, it can be tested if θ_{eq} falls in the expected range (Fig. 1). Cano et al. (2020) argues that mineral pairs of lunar rocks are not in equilibrium because the respective θ_{app} ranging from 0.47 to 0.56 are inconsistent with equilibrium. The respective range for terrestrial rocks (0.522 to 0.53) is generally more feasible, although the lowermost value is suspiciously low. The temperature determined by $^{18}\alpha_{A\text{-}B}$ dictates a given θ_{eq} typically >0.526 for high *T*. If this theoretical triple oxygen isotope exponent is not observed (within error), the mineral pair is not in equilibrium. Identifying disequilibrium for the hydrothermal quartz–epidote mineral pair (θ_{eq} = 0.526; Zakharov et al. 2019b) is outlined in more detail below, after introducing the basics of water–rock interaction.

WATER–ROCK INTERACTION

Hydrothermal alteration dominantly occurs in areas where hot magmatic rocks are cooled by the convective flow of fluids (Baumgartner and Valley 2001; Shanks 2001). Seawater penetrates the oceanic crust at the mid ocean ridges, resulting in large scale isotope exchange between the two reservoirs (Muehlenbachs and Clayton 1976; Sengupta and Pack 2018). Meteoric water with low $\delta^{18}O$ can imprint its isotopic composition on to rocks via fluid–rock interaction (Taylor 1978; Criss and Taylor 1983; Pope et al. 2014; Zakharov et al. 2019b). At high temperatures, the water to rock ratio (*W/R*) dictates if the isotopic composition of the rock is driven towards that of the water (high *W/R*) or if the water adjusts to the composition of the rock (low *W/R*). For magmatic and metamorphic waters, the rock usually governs the mass balance of the system, while in hydrothermal systems the constant flux of water dominates mass balance. In its simplest form, the *W/R* ratio is estimated via the mass balance of the mole fractions of the oxygen reservoirs in a closed system (Taylor 1978).

$$X_{rock} \times \delta^{i}_{rock} + \left(1 - X_{rock}\right)\delta^{i}_{water} = X_{rock} \times \delta^{f}_{rock} + \left(1 - X_{rock}\right)\delta^{f}_{water} \tag{10}$$

where X_{rock} is the mole fraction of oxygen in the rock and i and f stand for the initial and final compositions respectively. The *W/R* ratio is then:

$$\frac{W}{R} = \frac{\delta^{f}_{rock} - \delta^{i}_{rock}}{\delta^{i}_{water} - (\delta^{f}_{rock} - 1000 \ln \alpha_{rock-water})} \tag{11}$$

This equation applies to a batch system which is rarely true for hydrothermal systems. Therefore, "open system *W/R* ratios" are sometimes used:

$$\frac{W}{R} = \ln\left(\left(\frac{W}{R}\right)_{closed\ system} + 1\right) \tag{12}$$

Because the *W/R* ratio only accounts for the water that has actually reacted with the rock the meaning of *W/R* is not straight forward (see Baumgartner and Valley 2001 for a discussion). A full understanding of the transport and transformation rates and mechanisms is necessary (Putnis 2015; Druhan et al. 2019) to apply multi-dimensional transport models, which can be necessary to adequately model real world examples of water–rock exchange (Baumgartner and Valley 2001). In addition, other fluids than water are also relevant as addressed later in this chapter for CO_2 and SO_2. However, despite its simplicity, Equation (11) represents a good first order approximation to understand water–rock interaction.

To date, all ^{17}O studies on high temperature water–rock interaction are exclusively using this original definition (Herwartz et al. 2015; Zakharov et al. 2017, 2019a, b, 2021, this volume; Wostbrock et al. 2018; Sengupta and Pack 2018; Zakharov and Bindeman 2019; Wostbrock and Sharp 2021, this volume; Peters et al. 2020a, b; Chamberlain et al. 2020).

Combined $\delta^{18}O$ and δD isotope systematics are traditionally used to study water–rock interaction. Rocks comprise small mole fractions of hydrogen compared to oxygen, thus small quantities of water can significantly alter the δD, while $\delta^{18}O$ only changes at elevated *W/R*. Alteration trajectories in $\delta^{18}O$ vs. δD space are therefore strongly curved (Taylor 1978). In hydrothermal systems the aim is to resolve the intertwined effects of boiling, liquid–vapor phase separation, mixing and water–rock exchange at variable water–rock ratios and temperature (Shanks 2001; Pope et al. 2014). Additional $\delta^{17}O$ analyses help to resolve the individual processes and to extract information such as the initial fluid isotope composition of ancient seawater (Sengupta and Pack 2018; Zakharov and Bindeman 2019; Liljestrand et al. 2020; Peters er al. 2020b) or paleo-meteoric water providing insight into the respective hydrological cycles and thus climate (Herwartz et al. 2015; Zakharov et al. 2017, 2019a; Chamberlain et al. 2020). In the following section, I will show how the required parameters for the mass balance model can be constrained and how individual processes can be identified. The respective concepts could also be used to better understand contact metamorphism (Baumgartner and Valley 2001) or the genesis of mineral deposits (Shanks 2014), or any other field that presently uses the traditional $\delta^{18}O$ and δD isotope systematics.

Constraining input variables for the water–rock mass balance equation

For most hydrothermally altered rocks (with δ^{f}_{rock}) there are country rocks that have escaped water–rock interaction. Analyses of these pristine rocks, or average compositions for this rock type (e.g., MORB) closely resembles the initial rock isotopic composition (δ^{i}_{rock}) of the altered specimen.

The isotope fractionation between the bulk rock and water $1000 \ln \alpha_{rock–water}$ depends on its respective mineralogy and the temperature of water–rock interaction. For mixed mineralogy or for ancient samples, where the hydrothermal mineralogy is not preserved, typical bulk rock $1000 \ln \alpha_{rock–water} \approx 1–3‰$ are reasonable at typical hydrothermal temperatures and the $\delta^{17}O$ can be approximated via a high $\theta_{rock–water}$ around 0.526–0.53. For a preserved hydrothermal mineralogy, individual mineral fractionation factors can be used. Epidote for instance, typically forms at 250–400 °C with $1000 \ln {}^{18}\alpha_{epidote–H_2O} \approx 0‰$ at 400 °C and 1.5‰ at 250 °C (Zheng 1993; Bird and Spieler 2004). Such small fractionation factors allow to directly trace the final water isotopic composition (δ^{f}_{water}) in equilibrium with the altered rock (δ^{f}_{rock}) (Zakharov et al. 2019b).

The quartz–water fractionation at hydrothermal temperatures ($1000 \ln \alpha_{qz–H_2O}$) is several permill, hence the large fractionation between quartz and epidote can be utilized as geo-thermometer (Matthews 1994) that is accurate if the mineral pair forms in equilibrium. While equilibrium is generally observed (Zakharov et al. 2019b), disequilibrium is also expected to occur, simply because quartz forms over a much wider range of temperatures than epidote. If temperatures drop below the typical epidote stability field of > 250 °C, the driving force for water circulation (heat) decreases and effective *W/R* ratios are expected to decrease. Any quartz precipitated at this late stage does not form in equilibrium with epidote and comprises low $\Delta'^{17}O$ (Fig. 9). Intra mineral mixing (i.e., a bulk analysis) of two generations of quartz also decreases $\Delta'^{17}O$ (Zakharov and Bindeman 2019; Zakharov et al. 2019b) and thus "too low" $\theta_{qz–epidote}$ values are indicative of disequilibrium. Equilibrium $\theta_{epidote–H_2O} = \theta_{qz–H_2O} = 0.5278$ at 400 °C because $1000 \ln {}^{18}\alpha_{epidote–H_2O} \approx 0‰$. At 250°C the $\theta_{qz–H_2O} = 0.527$ (Sharp et al. 2016) and identical within error to an empirical $\theta_{qz–epidote} = 0.526 \pm 0.001$ estimate (Zakharov et al. 2019b). Any lower $\theta_{qz–epidote}$ reveals disequilibrium and respective temperature or δ^{f}_{water} estimates using quartz are inaccurate. Therefore, epidote more reliably captures δ^{f}_{water} during the main hydrothermal phase (Zakharov et al. 2019b).

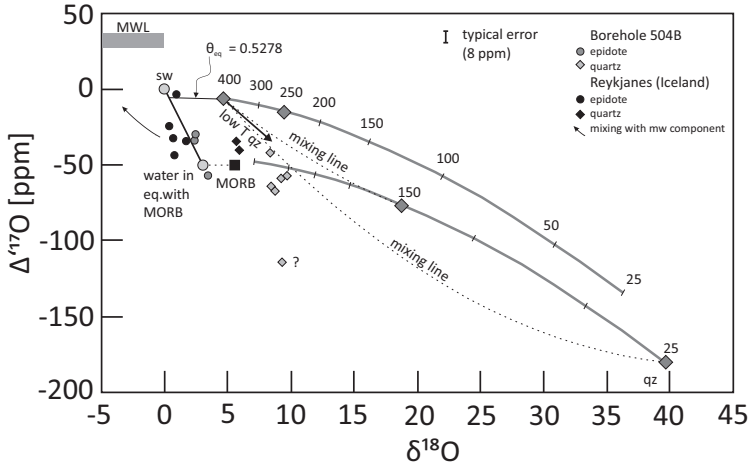

Figure 9. Triple oxygen isotope exchange during interaction between seawater and basalt. At high *W/R* ratios and hydrothermal temperatures epidote and quartz form in equilibrium with $\Delta'^{17}O$ close to zero. At 400 °C, epidote is isotopically identical to the water (Matthews et al. 1994), hence the $\theta_{quartz\text{-}epidote} = \theta_{quartz\text{–}water} = 0.5278$ (Sharp et al. 2016). Quartz precipitation during cooling and at low *W/R* has low $\Delta'^{17}O$. Intra-mineral mixing of high and low *T* precipitates (**stippled mixing curves**) drives $\Delta'^{17}O$ of bulk quartz to low values (**thick black arrow**). The apparent θ would decrease. The composition of epidote from Reykjanes is consistent with a meteoric water component at that site (**thin black arrow**); "Borehole 504B" is a marine site. The low $\Delta'^{17}O$ is only partially explained by late quartz precipitation at low *W/R*. Data is from Zakharov et al. (2019b) and Zakharov and Bindeman (2019).

Fluids from wells that penetrate active hydrothermal systems can be used to directly constrain δ^{f}_{water} of these high temperature systems. Water sampled from hot springs or geothermal power plants reveal ca. 40 ppm lower $\Delta'^{17}O$ for δ^{f}_{water} compared to δ^{i}_{water} (Wostbrock et al. 2018). In case of the Hellisheiði power plant in Iceland about 20% of the water is isotopically altered by water–rock interaction after passing through the hydrothermal pluming system (Wostbrock et al. 2018). Seawater derived fluids sampled from hydrothermal vents reveal that seawater-basalt reaction has little effect on δD and shifts $\delta^{18}O_{water}$ from near pristine values (≈0‰) at high *W/R* to ≈ 2‰ at low *W/R* ratios (Shanks 2001). Respective $\Delta'^{17}O$ decreases from near seawater compositions (i.e., –0.005‰; Luz and Barkan 2010) to mantle values (i.e., ≈ –0.05‰; Fig. 9) as confirmed by recent $\Delta'^{17}O$ analyses of high *T* altered oceanic crust and alteration products (Sengupta and Pack 2018). Both fluids and altered rocks evolve along trajectories with slopes of about 0.51 (Sengupta and Pack 2018; Zakharov et al. 2019b) that resemble mixing lines between the pristine and altered endmembers.

From $\delta^{18}O$ systematics alone it is impossible to calculate δ^{i}_{water} because the *W/R* ratio is generally unknown. The additional $\delta^{17}O$ analyses allow to extrapolate the mixing lines towards feasible δ^{i}_{water} compositions. Pristine fluids entering the crust (δ^{i}_{water}) are either seawater with δD, $\delta^{17}O$ and $\delta^{18}O$ all close to zero, or meteoric water with compositions close to the meteoric water line (MWL) with $\delta D = 8 \times \delta^{18}O + 10$ (Craig 1961; Dansgaard 1964) and $\delta'^{17}O = 0.528 \times \delta'^{18}O + 0.033$ (Luz and Barkan 2010). Global compilations of meteoric water actually reveal curved relationships (Li et al. 2015; Sharp et al. 2018; Surma et al. 2021, this volume), hence for individual studies it can be useful to define local meteoric water lines (LMWL), curves or intervals to approximate feasible combinations of δD, $\delta^{17}O$ and $\delta^{18}O$ for the pristine δ^{i}_{water}.

Constraining the isotopic composition of pristine (paleo-) fluids

Altered samples fall on a mixing line between the pristine endmember (δ^{i}_{rock}) and a hypothetical rock sample altered at infinite *W/R*, that is offset from the pristine δ^{i}_{water} by $1000\ln{}^{i}\alpha_{rock-water}$ (Fig. 6). Feasible compositions of the altered endmember fall on a line on or sub-parallel to the meteoric water line (depending on the $\theta_{rock-water}$). Extrapolating the mixing line defined by δ^{i}_{rock} and one or more altered samples (δ^{f}_{rock}) to this line (identical to the MWL herein; Fig. 6) gives the composition of the altered endmember at infinite *W/R*. The pristine δ^{i}_{water} is in equilibrium with this theoretical 100% alteration endmember, hence the calculated composition depends on the temperature of water–rock interaction.

Herwartz et al. (2015) tested this approach for samples from Krafla, Iceland and calculated rather low pristine $\delta^{18}O_{MW} = -22 \pm 4‰$ forcing the authors to speculate on a potential contribution of "ice age water" from the last glacial maximum. However, it is now clear that the $\Delta'^{17}O$ calibration between silicate samples relative to SMOW was inaccurate and that the scale was also rotated compared to the SMOW-SLAP scale (Pack and Herwartz 2014; Pack et al. 2016). Using a revised calibration of San Carlos olivine relative to SMOW from Pack et al. (2016) gives an intercept at −14‰ in perfect agreement with local meteoric water and consistent with directly measured well fluids and epidotes from the same site (Zakharov et al. 2019b). Herein, I also compensate for the "scale rotation" by recalibrating all data to a "mean SMOW-SLAP scale" (Table 1; supplementary data table), resulting in apparent $\delta^{18}O_{MW}$ ranging between −14 and −22‰ (Fig. 10) interpreted to represent some variation in the meteoric water isotopic composition over the timescales of water–rock interaction. Clearly, an accurate intercalibration between the water and silicate scale is critical in order to come to a robust interpretation for such datasets.

Traditionally, combined $\delta^{18}O$ and δD data are used in the same way (Taylor 1978; Criss and Taylor 1983; Pope et al. 2009). However, because the chemical behavior of oxygen differs from hydrogen and because hydrogen is susceptible to retrograde exchange at low temperatures (Savin and Lee 1988), combined $\delta^{18}O$ and δD datasets can be compromised. Chamberlain et al. (2020) analyzed triple oxygen and deuterium isotopes from hydrothermally altered rocks of the Idaho batholith. Paleo water $\delta^{18}O$ estimates derived from triple oxygen isotopes are higher than those derived from combined $\delta^{18}O$ and δD, which is interpreted as post crystallization exchange of hydrogen. The higher $\delta^{18}O_{MW}$ translates into a lower Eocene paleo elevation than originally proposed by Criss and Taylor (1983).

Especially for fossil analogue's to Iceland that have been metamorphosed, it can be difficult to interpret δD datasets (Bindeman and Serebryakov 2011; Zakharov et al. 2019a). By using additional $\delta^{17}O$ analyses, however, it is also possible to "see through" metamorphism and to constrain ancient $\delta^{18}O_{MW}$ compositions (Herwartz et al. 2015; Zakharov et al. 2019a).

Resolving the $\delta^{18}O$ composition of snowball Earth glaciers

Ice cores represent valuable climate archives because the measured $\delta^{18}O_{ice}$ can be translated into temperature using global or local $\delta^{18}O$ vs. *T* correlations (Dansgaard 1964; Masson-Delmotte et al. 2008). For the more distant past >1 Ma, the $\delta^{18}O$ of chemical sediments, especially carbonates are the most common temperature proxies (Zachos 2001). On an Earth that is entirely covered by ice, however, the atmosphere and the oceans are decoupled and isotopic temperature proxies are almost absent for these extreme climate states (Peng et al. 2013). Triple oxygen isotopes of hydrothermally altered rocks represent a rare exception.

Hydrothermal water–rock interaction was active throughout Earth's history, hence there are altered rocks that interacted with low $\delta^{18}O_{MW}$ meltwaters from ancient glaciers (Yui et al. 1995; Krylov 2007, 2008; Bindeman and Serebryakov 2011; Bindeman et al. 2014). The most prominent example are eclogites and ultra high pressure shists from the Dabie and Sulu terranes

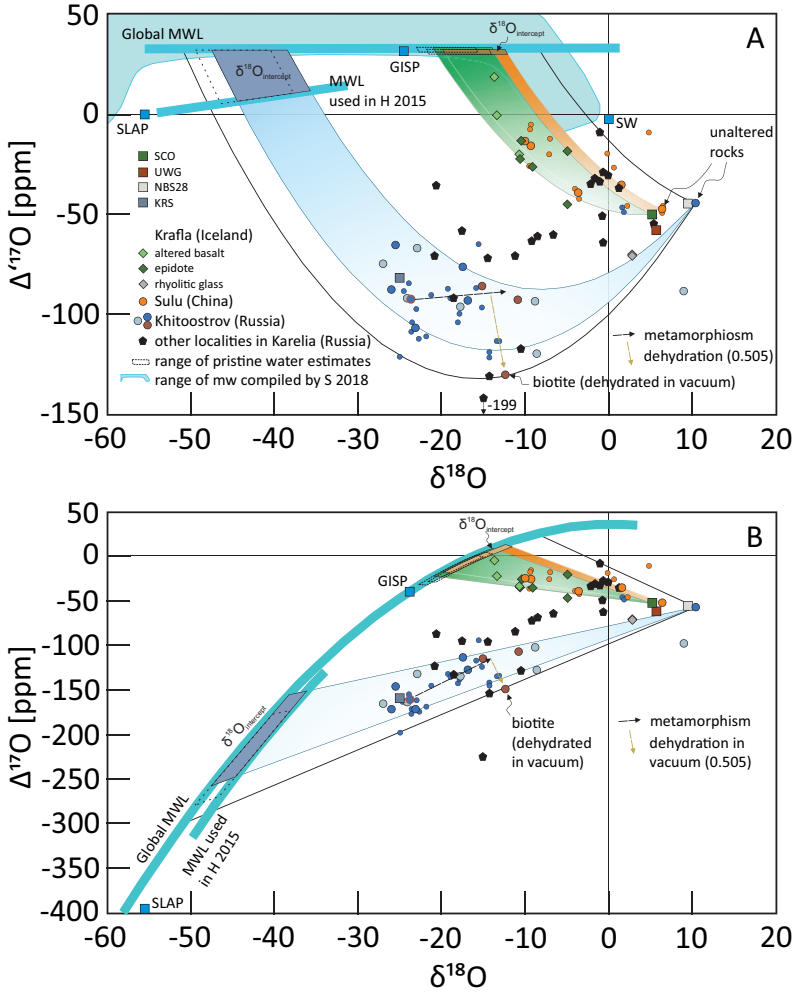

Figure 10. Hydrothermally altered rocks in triple oxygen isotope space. Data is presented on a linearized $\Delta'^{17}O$ (= $\delta'^{17}O - \lambda\delta'^{18}O$) vs. $\delta^{18}O$ scale in **Panel A** and on a traditional $\Delta^{17}O$ (= $\delta^{17}O - \lambda\delta^{18}O$) vs. $\delta^{18}O$ scale in Panel B. Mixing lines between the unaltered and altered rock are extrapolated to the global meteoric water line (which is a curve in **Panel B**). The intercepts represent the most feasible compositions for a hypothetical altered endmember in equilibrium with the pristine fluid. Hence, the fluid can be estimated from a respective $1000\ln{}^{i}\alpha_{rock-water}$ or $1000\ln{}^{i}\alpha_{mineral-water}$. Assuming a $\theta_{rock-water} = 0.528$ and a $1000\ln{}^{18}\alpha_{rock-water} = 2‰$ gives the stippled fields. Typical errors are 8 ppm SD for single analysis, hence the variation within individual sites probably reflects fluctuations in the meteoric water composition. Data from the "other localities" in Karelia including Mt. Dyadina, Kiy island, Varatskoe, Vaut Varakka, Height128 and Shueretskoe fluctuate even more representing strong climate fluctuations over the timescales of hydrothermal activity. Data are compiled from (Herwartz et al. 2015 (**dark blue** for Khitostrov); Zakharov et al. 2017, 2019a, b (**light blue** for Khitostrov) and normalized to SMOW-SLAP scale using standard values as reported in Table 1. The opposing absolute values reported for rock standards relative to SMOW and SLAP affect the calculated intercepts and thus the calculated composition of the pristine meteoric water. Using the SMOW-SLAP scale of Pack et al. (2016) increases calculated $\delta^{18}O_{MW}$ by ca. 1–2‰, while using the SMOW-SLAP scale from Wostbrock et al. (2020a) decreases calculated $\delta^{18}O_{MW}$ isotopic compositions by ca. 1–2‰. Metamorphism seems to drive minerals susceptible to alteration (biotite) back to higher $\delta^{18}O$ (**black stippled arrow**). Artificial dehydration of biotite by laser heating in vacuum drives the residual silicate to low $\Delta'^{17}O$, probably along a kinetic slope around 0.505 corresponding to dehydration (**yellow stippled arrow**; Clayton and Mayeda 2009).

in eastern China, which comprise $\delta^{18}O_{rock}$ as low as −10‰ (Yui et al. 1995). In triple oxygen isotope space, these samples fall on the "Iceland" trend implying that ancient water isotopic compositions had been similar to those in Iceland today or in the LGM (Herwartz et al. 2015). It is now thought that the respective water represents the Kaigas glaciation, a smaller event that followed the global Sturtian and Marinoan glaciations in the Neoproterozoic.

The most spectacular example of fossil hydrothermal vents known to date is observed for corundum bearing gneisses from the Belomorian belt in Karelia, northwestern Russia, which comprise $\delta^{18}O_{rock}$ down to ≈ −27‰ at the Khitoostrov locality (Krylov 2007, 2008; Bindeman and Serebryakov 2011; Bindeman et al. 2014). The respective water, which is thought to be associated to a Paleoproterozoic snowball Earth event at 2291 ± 8 Ma (Zakharov et al. 2017), must have had a $\delta^{18}O_{water}$ lower than −27‰, but it is impossible to say how much lower from the $\delta^{18}O$ systematics alone. Using triple oxygen isotope systematics, however, the $\delta^{18}O_{MW}$ can be approximated to ≈ −40‰ (Herwartz et al. 2015). In this case, the inaccurate calibration of the silicate vs. water scale (see above) has little effect on the result due to the strong curvature of the mixing line (Fig. 10). In a recent compilation (data from Herwartz et al. 2015; Zakharov et al. 2017, 2019a) on a revised reference frame, Zakharov et al. (2019a) determine an intercept at −38‰. After applying SMOW-SLAP normalization procedures (see above), intercepts for individual samples from Khitoostrov range from −35 to −47.5‰ translating to pristine glacial water isotopic compositions ranging between −35 and −50‰ for this locality (using $1000 \ln \alpha_{rock\text{-}water}$ from 0 to 2.5‰).

The observed scatter of the data is far larger than the analytical uncertainty. This variability is partly related to variable mineralogy and alteration temperatures. The main effect, however, is probably related to isotopic fluctuations in δ^{i}_{water}, related to climate fluctuations over the timescales of water–rock interaction. Sharp gradients in $\delta^{18}O_{MW}$ are expected for "snowball" or "slushball" Earth climate situations especially at low latitudes (Bindeman and Lee 2018). Hence, the mean $\delta^{18}O_{MW}$ ≈ −40‰ represents a mean value over the timescale of water–rock interaction with extremes down to −50‰ or less. Strongly variable $\delta^{18}O_{MW}$ between individual sites with $\delta^{18}O_{MW}$ up to ≈ −9‰ probably represent larger fluctuations on longer timescales (Zakharov et al. 2019a).

Direct U–Pb dating of the two local generations of gabbro intrusions to 2.43–2.41 Ga (high Mg gabbros) and 2.29 Ga (low Mg gabbros) suggest that two snowball Earth episodes are recorded in Karelia (Zakharov et al. 2017). Direct dating holds great potential for correlating glacial events recorded in hydrothermal rocks with diamictites from the Kola peninsula and more prominent diamictites from South Africa and Canada. Better age control allows better constraining the paleo-latitude of the ancient glaciers. It turns out that the Baltic Shield had been at near-equatorial to subtropical positions at the respective dates (Mertanen et al 1999; Salminen et al 2014) providing evidence for the extent of the ice cover (Bindeman et al. 2010; Zakharov et al. 2017).

It is tempting to translate the $\delta^{18}O_{MW}$ into mean annual temperatures using modern $\delta^{18}O_{MW}$ vs. *T* relationships (e.g., using MAT = $(\delta^{18}O_{MW} + 13.6)/0.69$; Dansgaard 1964), which implies that mean annual temperatures typical for Antarctica today persisted at tropical to (sub)tropical latitudes. Respective calibrations for glacial times (Jouzel et al. 1997; Lee et al. 2008) imply even lower temperatures and the isotope enabled Global Circulation Model reveals similar to modern $\delta^{18}O_{MW}$ vs. *T* relationships for very cold climate states (Bindeman and Lee 2018). The high $\delta^{18}O_{MW}$ ≈ −9‰ inferred for some sites in Karelia are consistent with strong climatic gradients expected especially for a "slushball" Earth (Bindeman and Lee 2018; Zakharov et al. 2019a) or for water–rock interaction unrelated to these extreme climate states.

Known occurrences of hydrothermal rocks altered by water derived from snowball earth glaciers are rare. Tephra and ignimbrite deposits also capture paleo meteoric water isotopic compositions especially when deposited directly on glacial ice (Hudak and Bindeman 2018). A detailed model for the respective triple oxygen isotope systematics (Rempel and Bindeman

2019), essentially comes down to mixing between a pristine and an altered endmember as outlined above. Rempel and Bindeman (2019) argue that tephra and ignimbrite deposits must have formed frequently during snowball earth events, providing another potential archive to study the hydrologic cycle of these enigmatic episodes in Earth history. However, interpreting ancient hydrosphere data requires accurate knowledge of ancient seawater compositions, since the ocean governs the mass balance of the hydrosphere.

Resolving the $\delta^{18}O$ composition of ancient seawater

Archean and Proterozoic chemical sediments have low $\delta^{18}O$ values compared to their modern analogues. For broadly similar ocean temperatures compared to today, this shift implies a shift in ocean water isotopic composition to values as low as −15‰ (Degens and Epstein 1962; Perry 1967; Jaffrés et al. 2007). From a ^{17}O perspective it now becomes clear that seawater $\delta^{18}O$ had not been very low (Sengupta and Pack 2018; Zakharov and Bindeman 2019; Hayles et al. 2020; Liljestrand et al. 2020; Peters et al. 2020b; Sengupta et al. 2020; Wostbrock and Sharp 2021, this volume; Zakharov et al. 2021, this volume).

The ocean water oxygen isotopic composition is argued to be at steady state with the Earth′s crust due to water–rock interaction at various temperatures (Muehlenbachs and Clayton 1976). The most important flux of exchanged oxygen is high-*T* alteration at mid ocean ridges, and the second most important fluxes are continental weathering and sea floor weathering at low temperatures. Together with "continental growth" and "water recycling", these fluxes control the oxygen isotopic composition of the modern and ancient ocean (Muehlenbachs and Clayton 1976; Gregory and Taylor 1981; Muehlenbachs 1986, 1998). Recent modelling in triple oxygen isotope space demonstrates that a low $\delta^{18}O$ ocean would have a high $\Delta'^{17}O$ (Sengupta and Pack 2018) which is inconsistent with Archean chert data (Levin et al. 2014) that fall below the present day quartz–water equilibrium curve of (Sharp et al. 2016). If the chert had formed in equilibrium with seawater at elevated temperatures, the triple oxygen isotopic composition would coincide with the equilibrium line, which is not the case (Sengupta and Pack 2018). Several datasets now support a diagenetic modification of the ancient chert (Degens and Epstein 1962), essentially representing a mixing process that drives $\Delta'^{17}O$ to lower values than expected both for equilibrium or a low $\delta^{18}O$ ocean (Sengupta and Pack 2018; Hayles et al. 2020; Liljestrand et al. 2020; Sengupta et al. 2020; Wostbrock and Sharp 2021, this volume; Zakharov et al. 2021, this volume).

An alternative approach is to study ancient oceanic crust that provides a record of high temperature water–rock interaction with seawater (Gregory and Taylor 1981). The same triple oxygen isotope systematics outlined above to derive the composition of ancient meteoric water (Herwartz et al. 2015) can also be used to approximate the composition of ancient seawater (Peters et al. 2020b). Serpentinites form via water–rock interaction of mafic rocks. Using petrological evidence and trace element systematics, Peters et al. (2020b) demonstrates that olivine from an ultramafic lens in the Archean Kuumiut terrane, Greenland formed via dehydration of serpentinite. Respective $\delta^{18}O_{olivine}$ are as low as 1.6‰ and ultimately derived from serpentinisation of peridotite with ancient seawater about 2.7 Ga ago. Triple oxygen isotope systematics of these samples is most consistent with water–rock interaction at 250 to 450 °C and an ancient seawater composition of $\delta^{18}O = -1$‰ typically assumed for Phanerozoic seawater (Peters et al. 2020b).

Zakharov and Bindeman (2019) directly investigated 2.42 Ga old submarine basalts from the Vetreny belt in Russia, that comprise pillow structures with preserved vein fillings of epidote, quartz and carbonate. Respective mineral pair equilibrium $\delta^{18}O$ temperatures range from 286 to 387°C, typical for hydrothermal temperatures, implying that the isotopic composition of these minerals is well preserved. Epidote almost directly captures water isotopic compositions and suggests a seawater $\delta^{18}O = -1.7 \pm 1.1$‰; $\Delta'^{17}O = -0.001 \pm 0.011$‰ and $\delta D = 0 \pm 20$‰ in the early Paleoproterozoic, consistent within error with modern ice free world seawater (Zakharov and Bindeman 2019).

All these studies suggest only slightly negative ancient $\delta^{18}O_{seawater}$ and only Bindeman (2021, this volume) still argues for moderately low $\delta^{18}O \approx -5$, based on shale data. Quantifying oxygen isotopic fluctuations of seawater through time will provide insight into the relative contributions of hydrothermal alteration and continental weathering.

RESOLVING INDIVIDUAL PROCESSES

In this section I review several processes that are potentially important when studying hydrothermal, igneous or metamorphic rocks. Resulting vectors in triple oxygen isotope space are summarized in Figure 11. These include: 1) boiling and phase separation; 2) assimilation; 3) CO_2 and SO_2 rich fluids; 4) decarbonation (including pyrolysis); 5) dehydration and; 6) alteration.

Boiling and phase separation observed in well fluids

At hydrothermal temperatures, the fractionation between liquid and vapor is small ($1000 \ln {}^{18}\alpha_{liquid-vapor} \approx 1‰$) and epidote data from Iceland implies that phase separation is generally not very important for the epidote forming hydrothermal fluids (Pope et al. 2009, 2012, 2014; Zakharov et al. 2019b). Hydrothermal water–rock interaction as discussed above precedes the boiling process, that only generates significant isotope effects at temperatures < 150 °C (Horita and Wesolowski 1994; Shmulovich et al. 1999). The respective $\theta_{liquid-vapor}$ is around 0.529 to 0.53 (Barkan and Luz 2005; Zakharov et al. 2019b) allowing to predict the triple oxygen isotope effects of boiling and phase separation of liquid and vapor in modern hydrothermal systems.

Well head fluids at Krafla (Iceland) are enriched in $\delta^{18}O$ and δD to a degree, which could be interpreted as water–rock interaction at low *W/R* ratios of ca. 0.2. Combined triple oxygen and hydrogen isotope systematics show, however, that a combined effect of water–rock interaction (*W/R* ≈ 2) and subsequent phase separation is required to explain well fluid isotopic compositions (Zakharov et al. 2019b). At Reykjanes (Iceland), mixing between seawater and meteoric water is an additional complication, but well fluids appear to be "too light" in δD implying that the vapor phase dominates the well fluids in this case (Arnórsson 1978; Pope et al. 2009; Zakharov et al. 2019b).

Assimilation of low $\delta^{18}O$ rocks

Magmatism drives hydrothermal systems and thus produces altered rocks in close proximity to the magma chamber. In regions with low $\delta^{18}O_{MW}$, such syn-eruptive alteration generates low $\delta^{18}O_{crust}$ that is assimilated by the magma generating low $\delta^{18}O$ magmatic rocks (Bindeman et al. 2012; Colón et al. 2015). For the classic example of Krafla on Iceland assimilation of altered country rock is estimated to around 10-20% using triple oxygen and hydrogen isotope mass balance (Elders et al. 2011; Zakharov et al. 2019b). The Scourie dikes from the Lewisian Complex in Scotland comprise negative $\delta^{18}O$, too low to be derived via assimilation of high-*T* altered oceanic crust. The most viable mechanism is assimilation of 20 to 30% of altered crust with very low $\delta^{18}O \approx -20$ to $-35‰$ similar to those found in Kithoostrov Karelia. Although this low $\delta^{18}O$ endmember has not been found anywhere in the area, the triple oxygen isotope data imply that the pristine meteoric water, that imprinted its isotopic composition onto the altered rocks, must have had $\delta^{18}O_{MW} \approx -35 \pm 10‰$ (Zakharov et al. 2019a). The close relationship of the Lewisian complex with the Belomorian belt lends support to this interpretation (Zakharov et al. 2019a).

The assimilation of country rocks into the magma chamber is traditionally studied using radiogenic or trace elements, but respective compositions differ substantially between altered and pristine rocks. Quantifying the amount of hydrothermally altered rock assimilated by a magma chamber via triple oxygen isotopes thus holds potential for a better interpretation of trace element and isotope data. Assimilation of other rock types such as carbonates or sulfates (Peters et al. 2020a) generate unique triple oxygen isotope trends that can aid in better quantifying specific lithologies assimilated by the magma. All vectors labeled as "mixing" in Figure 11 represent reasonable trajectories for assimilation.

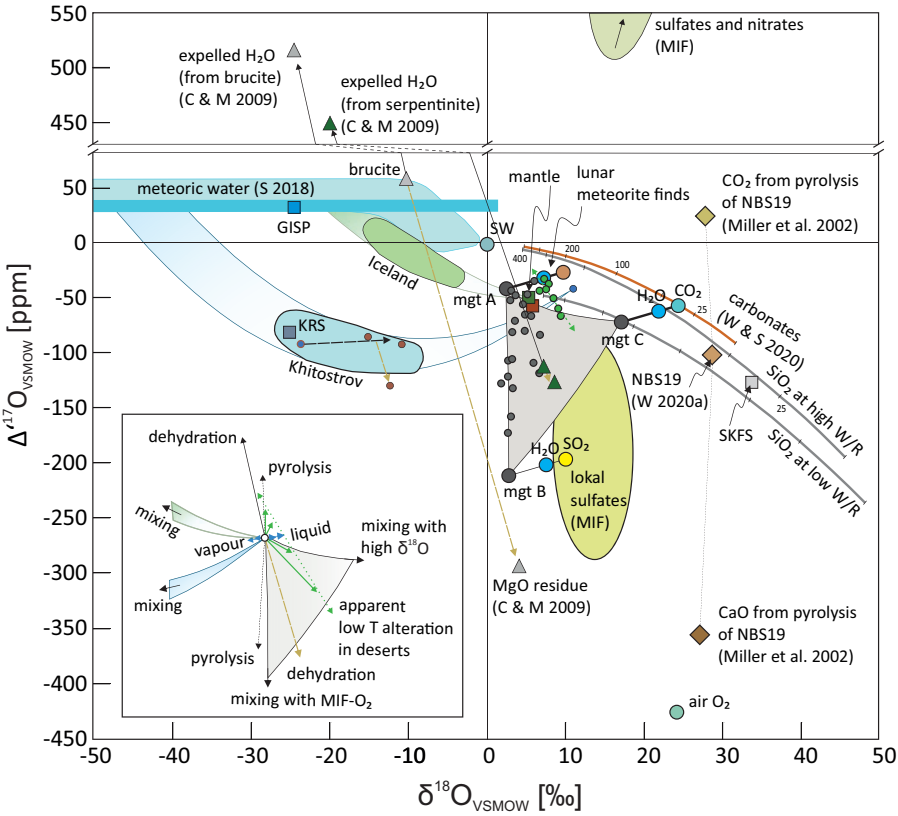

Figure 11. Summary of individual processes potentially affecting triple oxygen isotope compositions of crustal rocks. These include: 1) dehydration of serpentinite and brucite (Clayton and Mayeda 2009). For serpentinite (green triangles) the bulk composition is similar to the dehydrated phase, while mass balance forces the residual MgO to very low $\Delta'^{17}O$ for dehydration of brucite (**grey triangles**); 2) pyrolysis of carbonate (**brown diamonds**) using NBS19 as an example. Respective mean (and recalibrated) CaO and CO_2 data from (Miller 2002) are compared to bulk NBS19 data from Wostbrock et al. (2020a); 3) boiling and phase separation (**blue arrows** labeled "vapour" and "liquid" in the inset); 4) low *T* alteration of mafic rocks in desert environments is represented by lunar meteorite finds (supplementary dataset). These samples (**small green dots**) are altered at low *T* over thousands of years with evaporating water. The effective slope (**stippled green double arrow** with $\lambda = 0.5175$) of these samples does not pass through the unaltered endmember, because these samples weathered under variable climate conditions. Individual weathering trajectories (**green arrows** in the inset) probably had quite variable slopes. 5) precipitation of silicates (Sharp et al. 2016) and carbonates (Wostbrock and Sharp 2021, this volume) at variable temperatures and variable starting compositions for the water (i.e., seawater for carbonates and water equilibrated at variable *W/R* ratios with MORB for silicates); and 6) several mixing processes that can drive samples into various directions. Consider for instance mixing of magnetite A (formed in eq. with magmatic water), magnetite B (formed from fluids derived from sulfates with a negative MIF anomaly) and magnetite C (fromed from fluids with high X_{CO_2} derived from carbonates). These mixing endmembers explain measured magnetite compositions (**small dark grey dots**) within the **grey triangle** (Peters et al. 2020a). Mixing with light $\delta^{18}O$ altered endmembers (e.g., Iceland or Khitostrov) may drives samples in a completely different direction. Any contribution ultimately derived from atmospheric O_2 drives samples to low $\Delta'^{17}O$ (Pack et al. 2017; Pack 2021, this volume; Sutherland et al. 2020), while material ultimately derived from ozone (e.g., atmospheric sulfates and nitrates) increase $\Delta'^{17}O$ (Brinjikji and Lyons 2021, this volume; Cao and Bao 2021, this volume; Thiemens and Lin 2021, this volume;).

Isotopic exchange with CO_2 and SO_2

Assimilation and decomposition of carbonates or sulfates generate large quantities of CO_2 or SO_2. It is well known that the isotopic composition of H_2O can be modulated by equilibrium exchange with CO_2 in high X_{CO_2} fluids (Bottinga 1968; Truesdell 1974). High $\delta^{18}O_{magnetite}$ observed iron oxide deposits in Iran are probably derived from the CO_2 of decomposed Cambrian carbonates with $\delta^{18}O_{carbonate}$ = 20–30‰. In this particular case, exceptionally low $\Delta'^{17}O_{magnetite}$ compositions down to −170 ppm are also observed, which are probably inconsistent with mass dependent processes (Peters et al. 2020a). Local sulfates are known to comprise negative MIF signatures, which are apparently passed on to the magnetite ("mgt B" in Fig. 11). Formation temperatures of >800 °C (Troll et al. 2019) support a magmatic rather than a hydrothermal process. The natural MIF tracer of the sulfate rocks from the area (comprising low $\Delta'^{17}O_{SO_4}$) helps to distinguish between three viable endmembers (Fig. 11), demonstrating that SO_2 can significantly alter fluid isotopic compositions just like CO_2 (Peters et al. 2020a). The study also shows that minerals can capture and preserve transient fluid isotopic compositions, which may also be expected from large scale dehydration (Clayton and Mayeda 2009) and decarbonation (Miller et al. 2002) reactions.

Decarbonation

The reaction products derived from the thermal decomposition of carbonate ($CaCO_3 \rightarrow CaO + CO_2$) in vacuum differ by ≈ 400 ppm in $\Delta'^{17}O$ (Miller et al. 2002). This apparently mass independent process (see Fig. 11) is—to my knowledge—still not understood. Hence, it is unclear if thermal decomposition, which occurs on large scales in subduction zones, induces $\Delta'^{17}O$ heterogeneity. Fast re-equilibration with water and oxygen bearing minerals at temperatures >700 °C would rapidly diminish most of this initial $\Delta'^{17}O$, as also observed in experiments where the liberated CO_2 is not directly separated from solid CaO (Miller et al. 2002). However, a residual heterogeneity may be resolvable in natural systems at the present analytical precision.

Sun and Bao (2011b) proposed that the effect could be associated to a gas phase diffusion mechanism, related to the magnetic properties of ^{17}O affecting the effective collision diameter of respective isotopologues (Sun and Bao 2011a, b). These authors observe apparent mass independent fractionation in a thermal gradient for O_2 gas but not for oxygen in melts (Sun and Bao 2011a, b). Pyrolyses of $CaCO_3$ in melts does not seem to generate any "MIF" signature (Peters et al. 2020a) implying that the underlying process is indeed restricted to the gas phase.

Dehydration

The oxygen isotopic composition of hydroxyl groups and H_2O within a crystal lattice are generally distinct from other oxygen sites within a mineral (Zheng 1993; Girard and Savin 1996). This feature has been explored as a potential intra-mineral thermometer. Rapid dehydration under vacuum, with fast separation of the product water from the hot residual phase, generates large kinetic isotope fractionation effects that are superimposed on the intra-mineral fractionation. Dehydration of serpentinite, for instance, results in $\delta^{18}O_{water}$ that is ca. 15‰ lighter than the mineral internal $\delta^{18}O_{OH}$ that is in turn 19‰ lighter than non-hydroxyl oxygen (Clayton and Mayeda 2009). The large kinetic fractionation factors decrease to near zero (i.e., equilibrium) if the reaction products are not separated or heated to higher temperatures allowing for re-equilibration of the initial kinetic products with the anhydrous phases (Girard and Savin 1996).

Triple oxygen isotope slopes for the dehydration of serpentinite and brucite are 0.507 and 0.503 respectively (Clayton and Mayeda 2009). Both slopes are much shallower than expected for equilibrium θ ≈ 0.527 at 300°C (Fig. 1). The initial kinetic H_2O reaction products comprise average $\Delta'^{17}O_{rock-H_2O}$ = 570 ppm for the dehydration of serpentinite and as much as

$\Delta'^{17}O_{MgO–H_2O}$ = 810 ppm for dehydration of brucite (Fig. 11). In one analytical experiment, I dehydrated biotite via laser heating within the vacuum chamber of the fluorination line. The $\Delta'^{17}O$ of the residual silica glass came out 40 ppm lower compared to biotite fluorinated directly (Fig. 10), demonstrating that analytical protocols should be checked for such artefacts.

In this context it may be interesting to re-investigate the various techniques for the removal of exchangeable H_2O and OH from biogenic silica (Opal-A) prior to analyses (Chapligin et al. 2011; Bandriss et al. 1998). Most biogenic and abiogenic silica samples fall on the same curve in triple oxygen isotope space (Sharp et al. 2016; Wostbrock et al. 2018), but phytolith SiO_2 seems to have ca. 70 ppm lower $\Delta'^{17}O$ than expected (Alexandre et al. 2019), either reflecting kinetic processes during the SiO_2 polymerization, or contrasting isotopic effects for the respective dehydroxylation methods used (i.e., pre-fluorination vs. dehydration at 1000°C in a N_2 gas stream).

The fast re-equilibration kinetics observed for $\delta^{18}O$ (Girard and Savin 1996) imply that the preservation potential for such initial heterogeneity in $\Delta'^{17}O$ is limited on Earth. Peters et al. (2020b) does not observe a significant effect in olivine formed by dehydration of serpentinites. In this case, however, only a small mole fraction of the bulk oxygen is expelled as water. The maximum drawdown shift in $\Delta'^{17}O$ for the residual silicate is only 21ppm (Clayton and Mayeda 2009; Peters et al. 2020b; Fig. 11). For materials containing more hydroxyl groups such as brucite, dehydration may well leave a measurable $\Delta'^{17}O$ trace both in materials that react with the expelled water and in residual anhydrous phases. Preservation of the $\Delta'^{17}O$ requires fast separation of the expelled water at moderate temperatures, just high enough for the dehydration to proceed, but not too high as this would facilitate fast re-equilibration. Anhydrous minerals with low $\Delta'^{17}O$ would be generated, potentially explaining the surprisingly low $\Delta'^{17}O$ sporadically observed for quartz (Fig. 9), rhyolitic glass from Krafla and a few peculiar gneiss samples (Fig. 10). Alternatively, these minerals document mixing with extreme and yet unknown mixing components. Analytical artefacts related to dehydration prior analyses (see above) are not feasible for these nominally anhydrous minerals.

Dehydration into near-vacuum and fast separation of the initial kinetic water from the rock residue is far more feasible for extraterrestrial dehydration (or pyrolysis) reactions. It was shown that "metamorphosed carbonaceous chondrites" (MCCs) are probably genetically related to CM2 carbonaceous chondrite via multiple cycles of thermal processing including dehydration and rehydration of silicate phases (Clayton and Mayeda 2009; Ivanova et al. 2013). The proposed mechanism requires that the expelled water was at least not fully re-equilibrated, hence some of the apparently mass independent effects observed in extraterrestrial material may actually be derived from mass dependent processes. Heterogeneity in $\Delta'^{17}O$ between individual lunar lithologies and within green glass was assigned to a mass independent effect (Cano et al. 2020) but mass dependent mechanisms should not be excluded a priori. Dehydration of a magma fountain in vacuum would probably induce $\Delta'^{17}O_{green\ glass}$ heterogeneity provided that the magma was not completely anhydrous.

Alteration

Identifying and quantifying isotopic shifts related to alteration processes is a general challenge for using isotopes in earth sciences. Quantitative discussions of alteration related to cherts and carbonates are provided in recent triple oxygen isotope papers (Liljestrand et al. 2020; Zakharov et al. 2021, this volume; Wostbrock and Sharp 2021, this volume). Herein, I summarized how altered samples can be useful to learn about alteration endmembers that inform on paleo-environments. The assumption that apparent alteration trajectories always intersect the pristine endmembers must not be true, however, as evident from the following exotic example.

The alteration trend of lunar meteorite finds (supplementary dataset in Herwartz et al. 2014 recalibrated herein) does not intersect with pristine compositions ($\Delta'^{17}O \approx -50$ to -40 ppm at $\delta^{18}O \approx 5.5‰$) of lunar Apollo samples (e.g., Wiechert et al. 2001; Spicuzza et al. 2007; Hallis et al. 2010;

Herwartz et al. 2014; Young et al. 2016; Greenwood et al. 2018; Cano et al. 2020). The apparent alteration slope (stippled green double arrow in Fig. 11) plotted trough the samples (green dots in Fig. 11) is $\lambda = 0.5175$ and passes through $\Delta'^{17}O_{mantle} = -50$ ppm at $\delta^{18}O > 8‰$. Hence, the pristine endmember does not represent any endmember of this apparent alteration slope. Making that assumption would indicate a pristine lunar $\Delta'^{17}O$ composition that is >20 ppm higher compared to Earth's mantle, which is not the case (Wiechert et al. 2001; Spicuzza et al. 2007; Hallis et al. 2010; Herwartz et al. 2014; Young et al. 2016; Greenwood et al. 2018; Cano et al. 2020).

These samples are altered at low *T* over thousands of years with evaporating meteoric water. Therefore, low *T* alteration products inherit variable $\Delta'^{17}O$ ranging from freshwater (high $\Delta'^{17}O$) to evaporitic water (low $\Delta'^{17}O$). The average triple oxygen isotopic composition of this water strongly depends on the local climatic conditions (Surma et al. 2015, 2018, Herwartz et al. 2017; Gázquez et al. 2018, Voigt et al. 2020). Each individual meteorite interacted with a unique average water composition in a unique climate at a unique average temperature. All samples are displaced to higher $\delta^{18}O$, because the $1000 \ln \alpha_{\text{alteration product–}H_2O}$ are generally high and thus alteration endmembers generally comprise a high $\delta^{18}O$. The $\Delta'^{17}O_{\text{alteration product}}$ depends on the average alteration temperature, $\Delta'^{17}O_{water}$ and $\theta_{\text{alteration product–}H_2O}$. The alteration endmembers for the individual samples are probably strongly variable as indicated by the solid green arrows in the inset of Fig. 11. Hence, these samples are not expected to follow the same alteration trend and, the concept of plotting one slope through all samples is a misconception.

In this particular case, the samples share the same starting composition and they are all weathered in dry desert environments. Hence the overall trend with a low $\lambda = 0.5175$ could be related to mixing of residual evaporitic water in the rock with fresh meteoric water or fog as observed for source water in dry desert environments (Voigt et al. 2020), but the similarities in slope could also be a coincidence.

This exotic example of alteration may represent a good analogue for low *T* alteration of mafic rocks. More importantly, however, it shows how apparent alteration trajectories may deviate from expected relationships because the samples comprise some spatial and temporal variability. Assuming that the unaltered endmember must fall on a trend defined by a set of samples is clearly inaccurate in the above case. Whenever a certain isotopic variability in the pristine or alteration endmember is feasible, triple oxygen isotope compositions are expected to deviate from a uniform slope or mixing trajectory. In the case of Karelia outlined above, the respective variability of the samples was utilized to estimate variability in paleo water isotopic compositions.

CONCLUSIONS AND OUTLOOK

Triple oxygen isotope systematics provide a second dimension to the $\delta^{18}O$ scale. Extending traditional models built on $\delta^{18}O$ to $\delta^{17}O$ simply requires reasonable approximations for θ. The theoretical framework developed for $\delta^{18}O$ over the past decades can be adopted. The simplest application of additional $\delta^{17}O$ analyses is to test model assumptions such as equilibrium, which is crucial for palaeothermometry. A second application is to constrain parameters like *T*, *W/R* or δ^{i}_{water}, using the additional $\delta^{17}O$ quantity (Herwartz et al. 2015). Feasible sets of input parameters can be determined even for mathematically under constrained systems, specifying feasible approximations for individual parameters (Gázquez et al. 2018; Liljestrand et al. 2020). Unexpected $\delta^{17}O$ values may uncover processes or reaction components that had not been detected from the $\delta^{18}O$ systematics alone such as the role of SO_2 in the formation of magnetite (Peters et al. 2020a). Reaction kinetics dictate certain θ values, relating the triple oxygen isotopic compositions of educts and products in a unique way. Therefore, combined $\delta^{18}O$ and $\delta^{17}O$ analyses allow to test proposed reaction mechanisms and to study reaction rates (Cao and Bao 2017; Guo and Zhou 2019). High reaction rates and fast separation of the

reaction products is often realized in laboratories as summarized here for decarbonation and dehydration. Respective effects in $\Delta'^{17}O$ are quite significant and could be resolvable in natural high *T* environments as well. Being able to "see through" metamorphism (Herwartz et al. 2015) or diagenesis (Wostbrock and Sharp 2021, this volume) holds great potential for more accurate constraints on paleoenvironments if the expected variability for individual alteration endmebers is accounted for (lunar meteorite example).

This summary exhibits the potential of triple oxygen isotopes in more quantitatively constraining geological processes. The field of purely mass dependent ^{17}O systematics is rapidly expanding, but is still in a "tool development phase", especially with respect to igneous, metamorphic and hydrothermal rocks. Any field presently using $\delta^{18}O$ to study water–rock interaction will benefit from additional $\delta^{17}O$ analyses.

One of the greatest potentials is to reconstruct paleowater isotopic compositions. This is interesting for paleoclimate studies throughout Earth′s history, but especially for resolving long standing debates related to Precambrian hydrology. Accurate reconstructions for seawater and meteoric water provide a tool to investigate the hydrological cycle in deep time offering insights into paleoclimate and geodynamic regimes.

In this contribution I focused on silicates but other oxygen bearing materials such as carbonates, sulfates, phosphates, metal oxides etc. all comprise unique oxygen isotope systematics and thus characteristic $\delta^{18}O$ vs. $\Delta'^{17}O$ compositions that are unique to their respective formation mechanisms and conditions (Schauble and Young 2021, this volume).

ACKNOWLEDGEMENTS

I thank Andreas Pack and Ilya Bindeman for inviting me to write this chapter and for their editorial handling. Zach Sharp and David Zakharov provided excellent reviews that substantially improved the quality of this manuscript. I also thank Claudia Voigt and David Bajnai for their suggestions to improve the manuscript and Addi Bischoff for kindly providing the lunar meteorite samples. Financial support was provided by the DFG via Project HE 6357/2-1.

REFERENCES

Alexandre A, Webb E, Landais A, Piel C, Devidal S, Sonzogni C, Coupal M, Mazur JC, Pierre M, Prié F, Valle-Coulomb C, Outrequin C, Roy J (2019) Effects of leaf length and development stage on the triple oxygen isotope signature of grass leaf water and phytoliths: insights for a proxy of continental atmospheric humidity. Biogeosciences 16:4613–4625

Arnórsson S (1978) Major element chemistry of the geothermal sea-water at Reykjanes and Svartsengi, Iceland. Mineral Mag 42:209–220

Bajnai D, Guo W, Spötl C, Coplen TB, Methner K, Krsnik E, Gieschler E, Hansen M, Henkel D, Price GD, Raddatz J, Scholz D, Fiebig J (2020) Dual clumped isotope thermometry resolves kinetic biases in carbonate formation temperatures. Nature communications (accepted)

Bao H (2015) Sulfate: A time capsule for Earth′s O_2, O_3, and H_2O. Chem Geol 395:108–118

Bao H, Cao X, Hayles JA (2015) The confines of triple oxygen isotope exponents in elemental and complex mass-dependent processes. Geochim Cosmochim Acta 170:39–50

Barkan E, Luz B (2005) High precision measurements of $^{17}O/^{16}O$ and $^{18}O/^{16}O$ ratios in H_2O. Rapid Commun Mass Spectrom 19:3737–3742

Barkan E, Luz B (2007) Diffusivity fractionations of $H_2{}^{16}O/H_2{}^{17}O$ and $H_2{}^{16}O/H_2{}^{18}O$ in air and their implications for isotope hydrology. Rapid Commun Mass Spectrom 21:2999–3005

Baumgartner LP, Valley JW (2001) Stable isotope transport and contact metamorphic fluid flow. Rev Mineral Geochem 43:415–467

Beard BL, Handler RM, Scherer MM, Wu L, Czaja AD, Heimann A, Johnson CM (2010) Iron isotope fractionation between aqueous ferrous iron and goethite. Earth Planet Sci Lett 295:241–250

Beck WC, Grossman EL, Morse JW (2005) Experimental studies of oxygen isotope fractionation in the carbonic acid system at 15°, 25°, and 40°C. Geochim Cosmochim Acta 69:3493–3503

Bergel SJ, Barkan E, Stein M, Affek HP (2020) Carbonate ^{17}O excess as a paleo-hydrology proxy: Triple oxygen isotope fractionation between H_2O and biogenic aragonite, derived from freshwater mollusks. Geochim Cosmochim Acta 275:36–47

Bigeleisen J, Mayer MG (1947) Calculation of equilibrium constants for isotopic exchange reactions. J Chem Phys 15:261–267

Bigeleisen J, Wolfsberg M (1958) Theoretical and experimental aspects of isotope effects in chemical kinetics. *In:* Prigogine I, Debye P (eds) Advances in Chemical Physics. John Wiley & Sons, Inc., Hoboken, NJ, USA, pp 15–76

Bindeman IN (2021) Triple oxygen isotopes in evolving continental crust, granites, and clastic sediments. Rev Mineral Geochem 86:241–290

Bindeman IN, Serebryakov NS (2011) Geology, petrology and O and H isotope geochemistry of remarkably ^{18}O depleted Paleoproterozoic rocks of the Belomorian Belt, Karelia, Russia, attributed to global glaciation 2.4Ga. Earth Planet Sci Lett 306:163–174

Bindeman IN, Lee J-E (2018) The possibility of obtaining ultra-low-$\delta^{18}O$ signature of precipitation near equatorial latitudes during the Snowball Earth glaciation episodes. Precambrian Res 319:211–219

Bindeman IN, Schmitt AK, Evans DAD (2010) Limits of hydrosphere-lithosphere interaction: Origin of the lowest-known $\delta^{18}O$ silicate rock on Earth in the Paleoproterozoic Karelian rift. Geology 38:631–634

Bindeman I, Gurenko A, Carley T, Miller C, Martin E, Sigmarsson O (2012) Silicic magma petrogenesis in Iceland by remelting of hydrothermally altered crust based on oxygen isotope diversity and disequilibria between zircon and magma with implications for MORB: Silicic magma petrogenesis in Iceland. Terra Nova 24:227–232

Bindeman IN, Serebryakov NS, Schmitt AK, Vazquez JA, Guan Y, Azimov PY, Astafiev BY, Palandri J, Dobrzhinetskaya L (2014) Field and microanalytical isotopic investigation of ultradepleted in ^{18}O Paleoproterozoic "Slushball Earth" rocks from Karelia, Russia. Geosphere 10:308–339

Bird DK, Spieler AR (2004) Epidote in geothermal systems. Rev Mineral Geochem 56:235–300

Böttcher ME, Neubert N, Escher P, Von Allmen K, Samankassou E, Naegler TF (2018) Multi-isotope (Ba, C, O) partitioning during experimental carbonatization of a hyper-alkaline solution. Geochemistry 78:241–247

Bottinga Y (1968) Calculation of fractionation factors for carbon and oxygen isotopic exchange in the system calcite-carbon dioxide–water. J Phys Chem 72:800–808

Bottinga Y, Javoy M (1987) Comments on stable isotope geothermometry: the system quartz–water. Earth Planet Sci Lett 84:406–414

Brandriss ME, O'Neil JR, Edlund MB, Stoermer EF (1998) Oxygen isotope fractionation between diatomaceous silica and water. Geochim Cosmochim Acta 62:1119–1125

Brinjikji M, Lyons JR (2021) Mass-independent fractionation of oxygen isotopes in the atmosphere. Rev Mineral Geochem 86:197–216

Cano EJ, Sharp ZD, Shearer CK (2020) Distinct oxygen isotope compositions of the Earth and Moon. Nat Geosci

Cao X, Bao H (2021) Small triple oxygen isotope variations in sulfate: Mechanisms and applications. Rev Mineral Geochem 86:463–488

Cao X, Liu Y (2011) Equilibrium mass-dependent fractionation relationships for triple oxygen isotopes. Geochim Cosmochim Acta 75:7435–7445

Cao X, Bao H (2017) Redefining the utility of the three-isotope method. Geochim Cosmochim Acta 212:16–32

Cao X, Bao H, Gao C, Liu Y, Huang F, Peng Y, Zhang Y (2019) Triple oxygen isotope constraints on the origin of ocean island basalts. Acta Geochim 38:327–334

Chamberlain CP, Ibarra DE, Lloyd MK, Kukla T, Sjostrom D, Gao Y, Sharp ZD (2020) Triple oxygen isotope systematics of meteoric hydrothermal systems—implications for paleoaltimetry. Geochem Persp Lett 15:2026

Chapligin B, Leng ML, Webb E, Alexandre A, Dodd JP, Ijiri A, Lücke A, Shemesh A, Abelmann A, Herzschuh U, Longstaffe FJ, Meyer H, Moschen R, Okazaki Y, Rees NH, Sharp ZD, Sloane HJ, Sonzogni C, Swann GEA, Sylvestre F, Tyler JJ, Yam R (2011) Inter-laboratory comparison of oxygen isotope compositions from biogenic silica. Geochim Cosmochim Acta 75:7242–7256

Clark ID, Fontes JC, Fritz P (1992) Stable isotope disequilibria in travertine from high pH waters: Laboratory investigations and field observations from Oman. Geochim Cosmochim Acta 56:2041–2050

Clayton RN, Epstein S (1961) The use of oxygen isotopes in high-temperature geological thermometry. J Geol 69:447–452

Clayton RN, Mayeda TK (2009) Kinetic isotope effects in oxygen in the laboratory dehydration of magnesian minerals. J Phys Chem A 113:2212–2217

Clayton RN, O'Neil JR, Mayeda TK (1972) Oxygen isotope exchange between quartz and water. J Geophys Res 77:3057–3067

Clayton RN, Grossman L, Mayeda TK (1973) A component of primitive nuclear composition in carbonaceous meteorites. Science 182:485–488

Colón DP, Bindeman IN, Stern RA, Fisher CM (2015) Isotopically diverse rhyolites coeval with the Columbia River Flood Basalts: evidence for mantle plume interaction with the continental crust. Terra Nova 27:270–276

Coplen TB (2007) Calibration of the calcite–water oxygen-isotope geothermometer at Devils Hole, Nevada, a natural laboratory. Geochim Cosmochim Acta 71:3948–3957

Craig H (1961) Isotopic variations in meteoric waters. Science 133:1702–1703

Criss RE, Taylor HP Jr (1983) An $^{18}O/^{16}O$ and D/H study of Tertiary hydrothermal systems in the southern half of the Idaho batholith. GSA Bull 94:640–663
Daëron M, Drysdale RN, Peral M, Huyghe D, Blamart D, Coplen TB, Lartaud F, Zanchetta G (2019) Most Earth-surface calcites precipitate out of isotopic equilibrium. Nat Commun 10:429
Dansgaard W (1964) Stable isotopes in precipitation. Tellus 16:436–468
Dauphas N, Schauble EA (2016) Mass fractionation laws, mass-independent effects, and isotopic anomalies. Annu Rev Earth Planet Sci 44:709–783
Degens ET, Epstein S (1962) Relationship between O^{18}/O^{16} ratios in coexisting carbonates, cherts, and diatomites: geological notes. AAPG Bull 46:534–452
Devriendt LS, Watkins JM, McGregor H V. (2017) Oxygen isotope fractionation in the $CaCO_3$–DIC–H_2O system. Geochim Cosmochim Acta 214:115–142
Dietzel M, Usdowski E, Hoefs J (1992) Chemical and $^{13}C/^{12}C$-and $^{18}O/^{16}O$-isotope evolution of alkaline drainage waters and the precipitation of calcite. Appl Geochem 7:177–184
Dodson MH (1973) Closure temperature in cooling geochronological and petrological systems. Contrib Mineral Petrol 40:259–274
Druhan JL, Winnick MJ, Thullner M (2019) Stable isotope fractionation by transport and transformation. Rev Mineral Geochem 85:239–264
Elders WA, Friðleifsson GÓ, Zierenberg RA, Pope EC, Mortensen AK, Guðmundsson Á, Lowenstern JB, Marks NE, Owens L, Bird DK, Reed M (2011) Origin of a rhyolite that intruded a geothermal well while drilling at the Krafla volcano, Iceland. Geology 39:231–234
Elphick SC, Graham CM (1988) The effect of hydrogen on oxygen diffusion in quartz: evidence for fast proton transients? Nature 335:243–245
Epstein S, Buchsbaum R, Lowenstam H, Urey HC (1951) Carbonate–water isotopic temperature sclae. J Geol 62:417–426
Epstein S, Mayeda TK (1953) Variation in ^{18}O content of waters from natural sources. Geochim Cosmochim Acta 4:213–224
Evans NP, Bauska TK, Gázquez-Sánchez F, Brenner M, Curtis JH, Hodell DA (2018) Quantification of drought during the collapse of the classic Maya civilization. Science 361:498–501
Garlick GD, Epstein S (1967) Oxygen isotope ratios in coexisting minerals of regionally metamorphosed rocks. Geochim Cosmochim Acta 31:181–214
Gázquez F, Evans NP, Hodell DA (2017) Precise and accurate isotope fractionation factors ($\alpha^{17}O$, $\alpha^{18}O$, αD) for water and $CaSO_4 \times 2H_2O$ (gypsum). Geochim Cosmochim Acta 198:259–270
Gázquez F, Morellón M, Bauska T, Herwartz D, Surma J, Moreno A, Staubwasser M, Valero-Garcés B, Delgado-Huertas A, Hodell DA (2018) Triple oxygen and hydrogen isotopes of gypsum hydration water for quantitative paleo-humidity reconstruction. Earth Planet Sci Lett 481:177–188
Giletti BJ (1986) Diffusion effects on oxygen isotope temperatures of slowly cooled igneous and metamorphic rocks. Earth Planet Sci Lett 77:218–228
Girard J-P, Savin SM (1996) Intracrystalline fractionation of oxygen isotopes between hydroxyl and non-hydroxyl sites in kaolinite measured by thermal dehydroxylation and partial fluorination. Geochim Cosmochim Acta 60:469–487
Green M, Taube H(1963) Isotopic fractionation in the OH^-–H_2O exchange reaction. J Phys Chem 67:1565–1566
Greenwood RC, Barat JA, Miller MF, Anand M, Dauphas N, Franchi IA, Sillard P, Starkey NA (2018) Oxygen isotopic evidence for accretion of Earth's water before a high-energy Moon forming giant impact. Sci Adv 4:eaao5928
Gregory RT, Taylor HP (1981) An oxygen isotope profile in a section of cretaceous oceanic crust, Samail Ophiolite, Oman: evidence for $\delta^{18}O$ buffering of the oceans by deep (>5 km seawater hydrothermal circulation at mid-ocean ridges. J Geophys Res 84 (B4):2737–2755
Guo W, Zhou C (2019) Triple oxygen isotope fractionation in the DIC–H_2O–CO_2 system: A numerical framework and its implications. Geochim Cosmochim Acta 246:541–564
Hallis LJ, Anand M, Greenwood RC, Miller MF, Franchi IA, Russell SS (2010) The oxygen isotope composition, petrology and geochemistry of mare basalts: Evidence for large-scale compositional variation in the lunar mantle. Geochim Cosmochim Acta 74:6885–6899
Hayles JA, Cao X, Bao H (2016) The statistical mechanical basis of the triple isotope fractionation relationship. Geochem Perspect Lett 3:1–11
Hayles J, Gao C, Cao X, Liu Y, Bao H (2018) Theoretical calibration of the triple oxygen isotope thermometer. Geochim Cosmochim Acta 235:237–245
Hayles J, Yeung LY, Homann M, Banerjee A, Jiang H, Shen B, Lee CT (2020) Three billion year secular evolution of the triple oxygen isotope composition of marine chert. Submitted to Earth Planet Sci Lett; Non peer reviewed version available at EarthArXiv 10.31223/osf.io/n2p5q
Herwartz D, Pack A, Friedrichs B, Bischoff A (2014) Identification of the giant impactor Theia in lunar rocks. Science 344:1146–1150
Herwartz D, Pack A, Krylov D, Xiao Y, Muehlenbachs K, Sengupta S, Di Rocco T (2015) Revealing the climate of snowball Earth from $\Delta^{17}O$ systematics of hydrothermal rocks. PNAS 112:5337–5341
Herwartz D, Surma J, Voigt C, Assonov S, Staubwasser M (2017) Triple oxygen isotope systematics of structurally bonded water in gypsum. Geochim Cosmochim Acta 209:254–266

Hofmann MEG, Horváth B, Pack A (2012) Triple oxygen isotope equilibrium fractionation between carbon dioxide and water. Earth Planet Sci Lett 319–320:159–164
Horita J, Wesolowski DJ (1994) Liquid–vapor fractionation of oxygen and hydrogen isotopes of water from the freezing to the critical temperature. Geochim Cosmochim Acta 58:3425–3437
Hudak MR, Bindeman IN (2018) Conditions of pinnacle formation and glass hydration in cooling ignimbrite sheets from H and O isotope systematics at Crater Lake and the Valley of Ten Thousand Smokes. Earth Planet Sci Lett 500:56–66
Ivanova MA, Lorenz CA, Franchi IA, Bychkov AY, Post JE (2013) Experimental simulation of oxygen isotopic exchange in olivine and implication for the formation of metamorphosed carbonaceous chondrites. Meteorit Planet Sci 48:2059–2070
Jaffrés JBD, Shields GA, Wallmann K (2007) The oxygen isotope evolution of seawater: A critical review of a long-standing controversy and an improved geological water cycle model for the past 3.4 billion years. Earth-Sci Rev 83:83–122
Jouzel J, Alley RB, Cuffey KM, Dansgaard W, Grootes P, Hoffmann G, Johnsen SJ, Koster RD, Peel D, Shuman CA, Stievenard M (1997) Validity of the temperature reconstruction from water isotopes in ice cores. JGR Oceans 102(C12):26471–26487
Kim ST, O'Neil JR (1997) Equilibrium and nonequilibrium oxygen isotope effects in synthetic carbonates. Geochim Cosmochim Acta 61:3461–3475
Kohn MJ (1999) Why most "dry" rocks should cool "wet." Am Mineral 84:570–580
Krylov DP (2007) O^{18} depletion in corundum bearing rocks from North Karelija (the Baltic Shield). Water–rock Interact 7:87–89
Krylov DP (2008) Anomalous $^{18}O/^{16}O$ ratios in the corundum-bearing rocks of Khitostrov, northern Karelia. Dokl Earth Sci 419A:453–456
Landais A, Barkan E, Yakir D, Luz B (2006) The triple isotopic composition of oxygen in leaf water. Geochim Cosmochim Acta 70:4105–4115
Landais A, Steen-Larsen HC, Guillevic M, Masson-Delmotte V, Vinther B, Winkler R (2012) Triple isotopic composition of oxygen in surface snow and water vapor at NEEM (Greenland). Geochim Cosmochim Acta 77:304–316
Lazar C, Young ED, Manning CE (2012) Experimental determination of equilibrium nickel isotope fractionation between metal and silicate from 500°C to 950°C. Geochim Cosmochim Acta 86:276–295
Lee J-E, Fung I, DePaolo DJ, Otto-Bliesner B (2008) Water isotopes during the Last Glacial Maximum: New general circulation model calculations. J Geophys Res 113:D19109
Passey BH, Levin NE (2021) Triple oxygen isotopes in meteoric waters, carbonates, and biological apatites: implications for continental paleoclimate reconstruction. Rev Mineral Geochem 86:429-462
Levin NE, Raub TD, Dauphas N, Eiler JM (2014) Triple oxygen isotope variations in sedimentary rocks. Geochim Cosmochim Acta 139:173–189
Li S, Levin NE, Chesson LA (2015) Continental scale variation in ^{17}O-excess of meteoric waters in the United States. Geochim Cosmochim Acta 164:110–126
Liljestrand FL, Knoll AH, Tosca NJ, Cohen PA, Macdonald FA, Peng Y, Johnston DT (2020) The triple oxygen isotope composition of Precambrian chert. Earth Planet Sci Lett 537:116167
Liu T, Artacho E, Gázquez F, Walters G, Hodell D (2019) Prediction of equilibrium isotopic fractionation of the gypsum/bassanite/water system using first principles calculations. Geochim Cosmochim Acta 244:1–11
Luz B, Barkan E (2010) Variations of $^{17}O/^{16}O$ and $^{18}O/^{16}O$ in meteoric waters. Geochim Cosmochim Acta 74:6276–6286
Macris CA, Young ED, Manning CE (2013) Experimental determination of equilibrium magnesium isotope fractionation between spinel, forsterite, and magnesite from 600 to 800 °C. Geochim Cosmochim Acta 118:18–32
Masson-Delmotte V, Hou S, Ekaykin A, Jouzel J, Aristarain A, Bernardo RT, Bromwich D, Cattani O, Delmotte M, Falourd S, Frezzotti M (2008) A review of Antarctic surface snow isotopic composition: observations, atmospheric circulation, and isotopic modeling. J Clim 21:3359–3387
Matsuhisa Y, Goldsmith JR, Clayton RN (1978) Mechanisms of hydrothermal crystallization of quartz at 250°C and 15 kbar. Geochim Cosmochim Acta 42:173–182
Matthews A, Goldsmith JR, Clayton RN (1983) On the mechanisms and kinetics of oxygen isotope exchange in quartz and feldspars at elevated temperatures and pressures. Geol Soc Am Bull 94:396–412
Matthews A (1994) Oxygen isotope geothermometers for metamorphic rocks. J Metamorph Geol 12:211–219
Melander L, Saunders WH (1987) Reaction Rates of Isotopic Molecules. Robert E. (Ed.) Krieger Publishing Company: Malabar, FL
Mertanen S, Halls HC, Vuollo JI, Personen LJ, Stepanov VS (1999) Paleomagmatism of 2.44 Ga mafic dykes in Russia Karelia, eastern Fenoscandian Shield—implications for continental reconstructions. Prec Res 98:197–221
Miller MF, Pack A (2021) Why measure ^{17}O? Historical perspective, triple-isotope systematics and selected applications. Rev Mineral Geochem 86:1–34
Miller MF, Franchi IA, Thiemens MH, Jackson TL, Brack A, Kurat G, Pillinger CT (2002) Mass-independent fractionation of oxygen isotopes during thermal decomposition of carbonates. PNAS 99:10988–10993
Miller MF, Pack A, Bindeman IN, Greenwood RC (2020) Standardizing the reporting of $\Delta'^{17}O$ data from high precision oxygen triple-isotope ratio measurements of silicate rocks and minerals. Chem Geol 532:119332
Muehlenbachs K (1986) Alteration of the oceanic crust and the ^{18}O history of seawater. Rev Mineral Geochem 16:425–444

Muehlenbachs K (1998) The oxygen isotopic composition of the oceans, sediments and the seafloor. Chem Geol 145:263–273
Muehlenbachs K, Clayton RN (1976) Oxygen isotope composition of the oceanic crust and its bearing on seawater. J Geophys Res 81:4365–4369
Pack A (2021) Isotopic fingerprints of atmospheric molecular O_2 in rocks, minerals and melts. Rev Mineral Geochem 86:217–240
Pack A, Herwartz D (2014) The triple oxygen isotope composition of the Earth mantle and understanding $\Delta^{17}O$ variations in terrestrial rocks and minerals. Earth Planet Sci Lett 390:138–145
Pack A, Herwartz D (2015) Observation and interpretation of $\Delta^{17}O$ variations in terrestrial rocks - Response to the comment by Miller et al. on the paper by Pack and Herwartz (2014). Earth Planet Sci Lett 418:184–186
Pack A, Toulouse C, Przybilla R (2007) Determination of oxygen triple isotope ratios of silicates without cryogenic separation of NF_3—technique with application to analyses of technical O_2 gas and meteorite classification. Rapid Commun Mass Spectrom 21:3721–3728
Pack A, Tanaka R, Hering M, Sengupta S, Peters S, Nakamura E (2016) The oxygen isotope composition of San Carlos olivine on the VSMOW2-SLAP2 scale: San Carlos olivine on the VSMOW2-SLAP2 scale. Rapid Commun Mass Spectrom 30:1495–1504
Pack A, Höweling A, Hezel DC, Stefanak MT, Beck AK, Peters STM, Sengupta S, Herwartz D, Falco L (2017) Tracing the oxygen isotopic composition of the upper Earth′s atmosphere using cosmic spherules. Nat Comm 8:15702
Passey BH, Hu H, Ji H, Montanari S, Li S, Henkes GA, Levin NE (2014) Triple oxygen isotopes in biogenic and sedimentary carbonates. Geochim Cosmochim Acta 141:1–25
Peng Y, Bao H, Zhou C, Yuan X, Luo T (2013) Oxygen isotope composition of meltwater from a Neoproterozoic glaciation in South China. Geology 41:367–370
Perry EC (1967) The oxygen isotope chemistry of ancient cherts. Earth Planet Sci Lett 3:62–66
Peters ST, Alibabaie N, Pack A, McKibbin SJ, Raeisi D, Nayebi N, Torab F, Ireland T, Lehmann B (2020a) Triple oxygen isotope variations in magnetite from iron-oxidedeposits, central Iran, record magmatic fluid interaction with evaporite and carbonate host rocks. Geology 48:211–215
Peters STM, Szilas K, Sengupta S, Kirkland CL, Garbe-Schönberg D, Pack A (2020b) >2.7 Ga metamorphic peridotites from southeast Greenland record the oxygen isotope composition of Archean seawater. Earth Planet Sci Lett 544:116331
Pope EC, Bird DK, Arnórsson S, Fridriksson T, Elders WA, Fridleifsson GÓ (2009) Isotopic constraints on ice age fluids in active geothermal systems: Reykjanes, Iceland. Geochim Cosmochim Acta 73:4468–4488
Pope EC, Bird DK, Rosing MT (2012) Isotope composition and volume of Earth′s early oceans. PNAS 109:4371–4376
Pope EC, Bird DK, Arnórsson S (2014) Stable isotopes of hydrothermal minerals as tracers for geothermal fluids in Iceland. Geothermics 49:99–110
Putnis A (2015) Transient porosity resulting from fluid–mineral interaction and its consequences. Rev Mineral Geochem 80:1–23
Rempel AW, Bindeman IN (2019) A model for the development of stable isotopic water signatures of tephra deposited on ice following subglacial caldera collapse. J Volcanol Geotherm Res 377:131–145
Rumble D, Miller MF, Franchi IA, Greenwood RC (2007) Oxygen three-isotope fractionation lines in terrestrial silicate minerals: An inter-laboratory comparison of hydrothermal quartz and eclogitic garnet. Geochim Cosmochim Acta 71:3592–3600
Sade Z, Yam R, Shemesh A, Halvey I (2020) Kinetic fractionation of carbon and oxygen isotopes during $BaCO_3$ precipitation. Geochim Cosmochim Acta 280:395–422
Salminen J, Halls HC, Mertanen LJ, Personen J, Vuollo J, Söderlund U (2014) Paleomagnetic and geochronological studies on Paleoproterozoic diabase dykes of Karelia, East Finland - Key for testing the Superia supercraton. Precambrian Res 244:87–99
Savin SM, Lee M (1988) Isotopic studies of phyllosilicates. Rev Mineral Geochem 19:189–223
Schauble EA, Young ED (2021) Mass dependence of equilibrium oxygen isotope fractionation in carbonate, nitrate, oxide, perchlorate, phosphate, silicate, and sulfate minerals. Rev Mineral Geochem 86:137–178
Schoenemann SW, Schauer AJ, Steig EJ (2013) Measurement of SLAP2 and GISP $\delta^{17}O$ and proposed VSMOW-SLAP normalization for $\delta^{17}O$ and $^{17}O_{excess}$: Measurement of SLAP2 and GISP $\delta^{17}O$ values. Rapid Commun Mass Spectrom 27:582–590
Sengupta S, Pack A (2018) Triple oxygen isotope mass balance for the Earth′s oceans with application to Archean cherts. Chem Geol 495:18–26
Sengupta S, Peters STM, Reitner J, Duda JP, Pack A (2020) Triple oxygen isotopes of cherts through time. Chem Geol 554:119789
Shahar A, Young ED, Manning CE (2008) Equilibrium high-temperature Fe isotope fractionation between fayalite and magnetite: An experimental calibration. Earth Planet Sci Lett 268:330–338
Shahar A, Ziegler K, Young ED, Ricolleau A, Schauble EA, Fei Y (2009) Experimentally determined Si isotope fractionation between silicate and Fe metal and implications for Earth′s core formation. Earth Planet Sci Lett 288:228–234
Shanks WC (2001) Stable isotopes in seafloor hydrothermal systems: vent fluids, hydrothermal deposits, hydrothermal alteration, and microbial processes. Rev Mineral Geochem 43:469–525

Shanks WC (2014) Stable isotope geochemistry of mineral deposits. *In:* Treatise on Geochemistry. Elsevier, p 59–85
Sharp ZD, Wostbrock JAG (2021) Standardization of the triple oxygen isotope system: waters, silicates, carbonates, air and sulfate minerals. Rev Mineral Geochem 86:137–178
Sharp ZD, Gibbons JA, Maltsev O, Atudorei V, Pack A, Sengupta S, Shock EL, Knauth LP (2016) A calibration of the triple oxygen isotope fractionation in the SiO_2–H_2O system and applications to natural samples. Geochim Cosmochim Acta 186:105–119
Sharp ZD, Wostbrock JAG, Pack A (2018) Mass-dependent triple oxygen isotope variations in terrestrial materials. Geochem Persp Let 7:27–31
Shmulovich KI, Landwehr D, Simon K, Heinrich W (1999) Stable isotope fractionation between liquid and vapour in water–salt systems up to 600°C. Chem Geol 157:343–354
Sutherland KM, Wostbrock JAG, Hansel CM, Sharp ZD, Hein JR, Wankel SD (2020) Ferromanganese crusts as recorders of marine dissolved oxygen. Earth Planet Sci Lett 533:116057
Spicuzza MJ, Day JMD, Taylor LA, Valley JW (2007) Oxygen isotope constraints on the origin and differentiation of the Moon. Earth Planet Sci Lett 253:254–265
Starkey NA, Jackson CR, Greenwood RC, Parman S, Franchi IA, Jackson M, Fitton JG, Stuart FM, Kurz M, Larsen LM (2016) Triple oxygen isotopic composition of the high-$^3He/^4He$ mantle. Geochim Cosmochim Acta 176:227–238
Sun T, Bao H (2011a) Non-mass-dependent ^{17}O anomalies generated by a superimposed thermal gradient on a rarefied O_2 gas in a closed system. Rapid Commun Mass Spectrom 25:20–24
Sun T, Bao H (2011b) Thermal-gradient-induced non-mass-dependent isotope fractionation. Rapid Commun Mass Spectrom 25:765–773
Surma J, Assonov S, Herwartz D, Voigt C, Staubwasser M (2018) The evolution of ^{17}O-excess in surface water of the arid environment during recharge and evaporation. Sci Rep 8:4972
Surma J, Assonov S, Staubwasser M (2021) Triple oxygen isotope systematics in the hydrologic cycle. Rev Mineral Geochem 86:401–428
Tanaka R, Nakamura E (2013) Determination of ^{17}O-excess of terrestrial silicate/oxide minerals with respect to Vienna Standard Mean Ocean Water (VSMOW): ^{17}O-excess of terrestrial silicate/oxide minerals. Rapid Commun Mass Spectrom 27:285–297
Taylor (1978) Oxygen and hydrogen isotope studies of plutonic granitic rocks. Earth Planet Sci Lett 38:177–210
Thiemens MH, Lin M (2021) Discoveries of mass independent isotope effects in the Solar System: past, present and future. Rev Mineral Geochem 86:35–95
Thiemens MH, Heidenreich JE (1983) The mass-independent fractionation of oxygen: a novel isotope effect and its possible cosmochemical implications. Science 219:1073–1075
Troll VR, Weis FA, Jonsson E, Andersson UB, Majidi SA, Högdahl K, Harris C, Millet MA, Chinnasamy SS, Kooijman E, Nilsson KP (2019) Global Fe–O isotope correlation reveals magmatic origin of Kiruna-type apatite-iron-oxide ores. Nat Commun 10:1712
Truesdell AH (1974) Oxygen isotope activities and concentrations in aqueous salt solutions at elevated temperatures: Consequences for isotope geochemistry. Earth Planet Sci Lett 23:387–396
Urey HC (1947) The thermodynamic properties of isotopic substances. J Chem Soc 562–581
Voarintsoa NR, Barkan E, Bergel S, Vieten R, Affek HP (2020) Triple oxygen isotope fractionation between $CaCO_3$ and H_2O in inorganically precipitated calcite and aragonite. Chem Geol 539:119500
Voigt C, Herwartz D, Dorador C, Staubwasser M (2020) Triple oxygen isotope systematics of evaporation and mixing processes in a dynamic desert lake system. Hydrol Earth Syst Sci Discuss https://doi.org/10.5194/hess-2020-255
Wiechert U (2001) Oxygen isotopes and the Moon-forming giant impact. Science 294:345–348
Wostbrock JA, Sharp ZD, Sanchez-Yanez C, Reich M, van den Heuvel DB, Benning LG (2018) Calibration and application of silica-water triple oxygen isotope thermometry to geothermal systems in Iceland and Chile. Geochim Cosmochim Acta 234:84–97
Wostbrock JAG, Cano EJ, Sharp ZD (2020a) An internally consistent triple oxygen isotope calibration of standards for silicates, carbonates and air relative to VSMOW2 and SLAP2. Chem Geol 533:119432
Wostbrock JAG, Brand U, Coplen TB, Swart PK, Carlson SJ, Sharp ZD (2020b) Calibration of carbonate–water triple oxygen isotope fractionation: seeing through diagenesis in ancient carbonates. Geochim Cosmochim Acta 288:369–388
Wostbrock JAG, Sharp ZD (2021) Triple oxygen isotopes in silica–water and carbonate–water systems. Rev Mineral Geochem 86:367–400
Yeung L, Hayles JA (2021) Climbing the top of Mount Fuji: Uniting theory and observations of oxygen triple isotope systematics. Rev Mineral Geochem 86:97–135
Yeung LY, Hayles JA, Hu H, Ash JL, Sun T (2018) Scale distortion from pressure baselines as a source of inaccuracy in triple-isotope measurements. Rapid Commun Mass Spectrom 32:1811–1821
Young ED, Galy A, Nagahara H (2002) Kinetic and equilibrium mass-dependent isotope fractionation laws in nature and their geochemical and cosmochemical significance. Geochim Cosmochim Acta 66:1095–1104
Young ED, Kohl IE, Warren PH, Rubie DC, Jacobson SA, Morbidelli A (2016) Oxygen isotopic evidence for vigorous mixing during the Moon-forming giant impact. Science 351:493–496
Yui T-Fu, Rumble DIII, Lo C-H (1995) Unusually low $\delta^{18}O$ ultra-high-pressure metamorphic rocks from the Sulu Terrain, eastern China. Geochim Cosmochim Acta 59:2859–2864

Zachos J (2001) Trends, rhythms, and aberrations in global climate 65 Ma to present. Science 292:686–693
Zakharov DO, Bindeman IN (2019) Triple oxygen and hydrogen isotopic study of hydrothermally altered rocks from the 2.43–2.41 Ga Vetreny belt, Russia: An insight into the early Paleoproterozoic seawater. Geochim Cosmochim Acta 248:185–209
Zakharov DO, Bindeman IN, Slabunov AI, Ovtcharova M, Coble MA, Serebryakov NS, Schaltegger U (2017) Dating the Paleoproterozoic snowball Earth glaciations using contemporaneous subglacial hydrothermal systems. Geology 45:667–670
Zakharov DO, Bindeman IN, Serebryakov NS, Prave AR, Azimov PY, Babarina II (2019a) Low $\delta^{18}O$ rocks in the Belomorian belt, NW Russia, and Scourie dikes, NW Scotland: A record of ancient meteoric water captured by the early Paleoproterozoic global mafic magmatism. Precambrian Res 333:105431
Zakharov DO, Bindeman IN, Tanaka R, Friðleifsson GÓ, Reed MH, Hampton RL (2019b) Triple oxygen isotope systematics as a tracer of fluids in the crust: A study from modern geothermal systems of Iceland. Chem Geol 530:119312
Zakharov DO, Marin-Carbonne J, Alleon J, Bindeman IN (2021) Triple oxygen isotope trend recorded by Precambrian cherts: A perspective from combined bulk and in situ secondary ion probe measurements. Rev Mineral Geochem 86:323–365
Zeebe RE (2014) Kinetic fractionation of carbon and oxygen isotopes during hydration of carbon dioxide. Geochim Cosmochim Acta 139:540–552
Zheng Y-F (1993) Calculation of oxygen isotope fractionation in anhydrous silicate minerals. Geochim Cosmochim Acta 57:1079–1091